

Application of a SPH depth-integrated model to landslide run-out analysis

Abstract Hazard and risk assessment of landslides with potentially long run-out is becoming more and more important. Numerical tools exploiting different constitutive models, initial data and numerical solution techniques are important for making the expert's assessment more objective, even though they cannot substitute for the expert's understanding of the site-specific conditions and the involved processes. This paper presents a depth-integrated model accounting for pore water pressure dissipation and applications both to real events and problems for which analytical solutions exist. The main ingredients are: (i) The mathematical model, which includes pore pressure dissipation as an additional equation. This makes possible to model flowslide problems with a high mobility at the beginning, the landslide mass coming to rest once pore water pressures dissipate. (ii) The rheological models describing basal friction: Bingham, frictional, Voellmy and cohesive-frictional viscous models. (iii) We have implemented simple erosion laws, providing a comparison between the approaches of Egashira, Hungr and Blanc. (iv) We propose a Lagrangian SPH model to discretize the equations, including pore water pressure information associated to the moving SPH nodes.

Keywords Rock-debris avalanches · Run-out · Numerical modelling · Rheological modelling · Depth-integrated models

Introduction

The run-out stage of fast-moving landslides (e.g. debris flows, debris and rock avalanches, flowslides, mudflows) and the problems encountered when trying to model this type of phenomenon complicate hazard zonation in many mountainous areas. These very rapid to extremely rapid phenomena are characterized by flow-like motion of materials with very varied and mutable properties. Abundance of coarse and fine particles, as well as water saturation may vary widely among the different types of movement, and they can control the mechanism of transport and material entrainment, the landslide dynamics, the occurrence of surges, and the final deposit characteristics. The state of effective stress, which controls slope deformation, stability and the eventual rapid evolution varies in time because of changes in the applied stresses (e.g. by earthquakes external loading, water impounding), pore pressures (e.g. by groundwater table recharge), material properties (e.g. weathering, water content, temperature), and geometry (e.g. erosion, excavation).

In order to accomplish a Quantitative Risk Analysis (QRA) for long-run-out landslides, different models with different accuracies are currently used (Fell et al. 2008). While some of them are still at the research stage, others have been thoroughly tested and used, as in the case of depth-integrated models. This paper focuses on rational models of continuum type because they can be applied to a large variety of problems. We do not consider here the discrete element models, because so far they can be applied prevalently to

dry rock avalanches with limitations presently linked to the maximum number of particles that can reasonably be simulated.

Continuum models are formulated mathematically as a set of coupled non-linear partial differential equations. The traditional approach for numerically solving these equations is by means of discretization in both time and on a spatial grid. A wide variety of such models have been developed over the past decades, and they have had impressive success in modelling controlled laboratory experiments with granular materials and—arguably to a lesser degree—natural gravity mass flows (mainly because the complex material behavior is not adequately captured in the mathematical models). However, these simulations usually start only *after* failure. In fact, numerical techniques based on fixed or moving meshes are poorly suited for simulating processes like formation of shear bands and break-up (even though they can be coerced to do so). Meshless methods, such as the Material Point Method (MPM) or Smoothed Particle Hydrodynamics (SPH), offer a more natural way of modelling both the initiation and the propagation stages of landslides in a consistent manner. We will concentrate on SPH techniques even though other methods exist. As a consequence, this contribution does not aim to be a comprehensive review of the existing models and approaches presented in the vast literature regarding this specific subject, but some pointers to alternative approaches are given in “A brief state-of-the-art of run-out models” in order to set the presented model into its context.

A brief state-of-the-art of run-out models

In general, one can broadly classify the different methods for modelling the run-out of fast-moving landslides (sometimes termed flow-like landslides) as either empirical or rational. Models from the former group are used to estimate travel distances rather than to provide quantitative values of the most important variables (e.g. velocity, thickness, movement direction). They may be based on geometrical relationships between the slope and the landslide deposits (Lied and Bakkehoi 1980; Hungr and Evans 1988; Evans and Hungr 1993; Corominas 1996; Iverson et al. 1998; Hunter and Fell 2003; Hungr et al. 2005; Crosta et al. 2003) or on volume change methods (Cannon 1993; Fannin and Wise 2001). In general, these relationships are established starting from a series of field observations of past events, which should be well differentiated and classified on the basis of different controlling factors (e.g. lithology, presence of water, ice or snow, degree of topographic confinement, geometry of the slope profile, erosion and bulking up).

On the other hand, rational methods are based on the use of mathematical models of different degrees of complexity and can be classified as follows:

- (a) *Discrete models.* They are used where the granularity of the moving mass is important. The simplest case is that of a block falling along a slope, with a geometry that can be modelled

with precision or approximated. The model checks for impacts with the topographic surface applying a suitable impact model (e.g. Agliardi and Crosta 2003).

On the other end of the spectrum, discrete elements have been used to simulate rock avalanches. The avalanche is approximated by a set of particles of simple geometrical forms (disks/cylinders, spheres) with ad hoc laws describing the contact forces. The number of material parameters is rather small (friction, sometimes an initial cohesion, and elastic contact properties). In many cases, it is not feasible to reproduce all the blocks of the avalanche, which is therefore approximated with a smaller number of blocks (as the contact forces are size-dependent, one needs to calibrate the model differently, however). The spheres (3D) or disks (2D) can be combined to form more complex shapes, and given granulometries can be generated. One main advantage of these methods is their ability to reproduce effects far beyond the reach of continuum models (Taboada and Estrada 2009), such as inverse segregation (Calvetti et al. 2000) or grain breakage.

Discrete element models are suitable for the simulation of rock avalanches, but for the time being we do not recommend using them in other situations (e.g. flowslides, lahars, mudflows) because the rheology of some (flowing) materials is not adequately rendered by colliding particles only. While inclusion of the fluid-grain coupling is possible (by CFD and DEM codes) in principle, the computational costs are still prohibitive.

- (b) *Continuum models.* They are based on continuum mechanics, and can include coupling of the mechanical, hydraulic and thermo-mechanical behaviour. The following subgroups may be distinguished:
- (b.1) *3D models based on mixture theory.* The most complex model category involves all phases that can be present in the flowing material, i.e. solid particles, fluid and gas. The relative displacements of the phases can be large, so that this group of models can be applied to the most general case. However, due to the great number of unknowns and equations, these models have not been used except when mixture effects are of paramount importance, which may be the case for mudflows and some rock-debris avalanches. As the geometry and the physics are rather complex, no analytical solutions exist and it is necessary to solve the equations using a suitable numerical model, such as finite elements or SPH. These models are very expensive in terms of computing time, but have to be used in situations where 3D effects are important, as in the case of impulse waves generated by landslides (Quecedo et al. 2004) or impact of the flowing material on structures and buildings. 3D models, are, in our opinion, the basis of a future generation of models describing all existing fluid and solid phases and their interactions. The mathematical formulation is already available (Pitman and Le 2005; Pudasaini and Hutter 2007; Zienkiewicz and Shiomi 1984). However, much effort is still needed in developing efficient computer codes.

- (b.2) *Velocity-pressure models (Biot–Zienkiewicz).* In many situations, the movement of pore fluids relative to the soil skeleton can be assumed to be small, and the model can be cast in terms of the velocity of the solid particles and the pore pressures of the interstitial fluids. This is the classical approach used in geotechnical engineering. Biot's approach (1941, 1955) for linear elastic materials was extended to non-linear materials and large deformation problems by Zienkiewicz and co-workers (1980; Zienkiewicz and Shiomi 1984; Zienkiewicz et al. 1990a, b, 2000), Lewis and Schrefler (1998), Coussy (1995) and de Boer (2000). Coupled formulations are now widely used in geotechnics to describe the behaviour of foundations and geostructures, failure of earth dams, slope failures and landslide triggering mechanisms. Again, the resulting model is 3D, and the computational effort to solve it is large. Material Point Method (MPM), Smoothed Particle Hydrodynamics (SPH), and Arbitrary Lagrangian-Eulerian (ALE) methods, such as demonstrated by Crosta et al. (2008), can be used. Their field of application is presently restricted to slides with short to medium run-out because of the required computational effort, but they have the advantage that pore pressures can be fully described.

The main interest of velocity pressure models is to characterize the triggering mechanism, providing initial conditions (landslide mobilized mass and basal pore pressures) which can be used in the propagation analysis

- (b.3) *Depth-integrated models.* Because of the geometry of the majority of fast-propagating landslides (i.e. low depth to length ratio, implying a small vertical velocity component; particles smaller than flow depth), it is possible to use a depth integration approximation. The equations reduce from 3D to 2D, as all variables depend only on x and y , the information on z -dependence being lost in the integration procedure. This method has been classically used in hydraulics and coastal engineering (e.g. flow in channels, long waves, tides). In the context of gravity mass flows, they were introduced by Eglit, Grigorian and co-workers in the 1960s (Briukhanov et al. 1967). Since then, especially after Savage and Hutter (1989, 1991), they have been widely used by engineers and earth scientists. The method allows to include information on the basal pore pressure, as done by Iverson and Denlinger 2001 and Pastor et al. (2009a), levees deposition and entrainment (Mangeney et al. 2007a, b; Johnson et al. 2012; Iverson 2012) and can be extended to two-phase models (Pitman and Le 2005; Pudasaini 2012; Pelanti et al. 2008). The pressures and forces on structures obtained in depth-integrated models are not fully correct, because of limited information on vertical profiles of velocities. For more reliable results, it is necessary to couple the 2D depth-integrated models with a local fully 3D model, where: the depth-integrated

model is used to simulate the entire flow to provide appropriate initial conditions for the 3D simulation in the proximity of the obstacle.

Concerning segregation, the problem has been studied and continuum models have been formulated by several researchers during the past years, such as Vallance and Savage (2000), Trujillo and Herrmann (2003), Gray and Thornton (2005), Gray and Ancey (2011) and Johnson et al. (2012). In the case of grain breaking, Iverson et al. (2010) have suggested that it can generate pore pressures during landslide propagation. They studied the behaviour of a loamy sand presenting aggregates in a shear ring apparatus, concluding that the breaking of aggregates caused a tendency to compact and, hence, increase of pore pressures. Constitutive and numerical analysis of crushing has been studied by Daouadji and Hicher (2010), Hu et al. (2012), Kikumoto et al. (2009), and Russell et al. (2009).

Depth-integrated models provide an excellent compromise between computer time and accuracy. They have been used to describe rock avalanches, lahars, mudflows, debris flows, flowslides and snow avalanches (see for example McDougall and Hungr 2004; Sosio et al. 2011, 2012).

- (b.4) Depth-integrated models can be simplified, as in the case of the so-called *infinite landslide approaches*. Indeed, the block analysis performed in many cases consists of a succession of infinite landslides evolving over a variable topography, where pore pressure dissipation can be included (e.g. Hutchinson 1986). Block models have been improved in order to consider the kinematics of several blocks interacting with each other, including thermo-dynamical effects (Pinyol and Alonso 2010; Alonso and Pinyol 2010).

The interest of the infinite landslide model comes from the fact that many of the basal friction laws are derived from general 3D rheological models in a consistent manner. The method consists of obtaining a velocity profile from which both the basal friction and the averaged velocity are obtained. Then, it is possible to relate both terms, obtaining the friction as a function of the depth-averaged velocity.

Behaviour of fluidized soils: alternatives for rheological modelling

As mentioned above, through depth integration we lose information about the flow structure along the slope-perpendicular direction, which is needed to obtain both the basal friction and the depth-integrated stress tensor. A widely used solution assumes that the flow at a given point and time, with known depth and depth-averaged velocities, has the same vertical structure as a uniform, steady-state flow. In the case of flow-like landslides this model is often referred to as the infinite landslide, as it is assumed to have constant depth and to move at constant velocity along a constant slope. This infinite landslide model is used to obtain approximate values for crucial quantities in our depth-integrated model. We will present next some rheological models frequently found in landslide propagation modelling.

Bingham fluid

The Bingham fluid is perhaps the simplest example of a rheological relation that exhibits transition between solid and fluid states. As long as the shear stress does not exceed a threshold τ_Y specific to the material, the latter behaves as a solid. Where the threshold is exceeded, the material flows like a Newtonian fluid. In the simple case of plane shear, the rheological relation is formulated in terms of the shear rate and the shear stress τ as

$$\dot{\gamma} = \text{sgn}(\tau) \Theta(|\tau| - \tau_Y) \frac{|\tau| - \tau_Y}{\mu} \quad (1)$$

where the Heaviside function $\Theta(x) = 1$ if $x > 0$ and 0 otherwise, $v(x, t)$ is the local flow velocity and μ is the (Bingham) viscosity. In the infinite-slope approximation, the problem of a uniform layer of (sufficiently large) depth h flowing on a plane inclined at an angle θ has the following stationary solution:

$$v(z) = \begin{cases} v_p \left[1 - \left(1 - \frac{z}{h_s} \right)^2 \right], & 0 \leq z < h_s \\ v_p, & h_s \leq z \leq h_p \end{cases} \quad (2)$$

with $h_p = \frac{\tau_Y}{\rho g \sin(\theta)}$ the depth of the unsheared, quasi-solid top layer ("plug layer") and $h_s = h - h_p$ the shear layer depth. The velocity of the plug layer is given by

$$v_p = \frac{\rho g h \sin \theta - \tau_Y}{2\mu} h_s = \frac{1}{2} \frac{\tau_B h}{\mu} \left(1 - \frac{\tau_Y}{\tau_B} \right)^2 \quad (3)$$

$\tau_B = \rho g h \sin \theta$ is the bed shear stress. In the case of Bingham fluids, there exists an additional difficulty, because it is not possible to obtain directly in a simple manner the shear stress at the bottom as a function of the averaged velocity. In fact, the expression relating the averaged velocity to the basal friction for the infinite landslide problem is

$$\bar{v} = \frac{\tau_B h}{6\mu} \left(1 - \frac{\tau_Y}{\tau_B} \right)^2 \left(2 + \frac{\tau_Y}{\tau_B} \right) \quad (4)$$

where μ is the viscosity, τ_Y the yield stress, and τ_B the shear stress at the bottom. This expression can be transformed into

$$P_3(\eta) := \eta^3 - (3 + a)\eta + 2 = 0 \quad (5)$$

where we have introduced $\eta = h_p/h$, the ratio between the height of the constant velocity region or plug to the total height of the flow, and the non-dimensional number a defined as

$$a = \frac{6\mu \bar{v}}{h \tau_Y} \quad (6)$$

It is thus necessary to obtain the root of a third-order polynomial. To decrease the computational load, several simplified solutions have been proposed. Pastor et al. (2004) introduced a simple method based on obtaining the second order polynomial, which represents the best approximation to the third-order polynomial which is given by

$$P_2(\eta) = \frac{3}{2} \eta^2 - \left(\frac{57}{16} + a \right) \eta + \frac{65}{32} \quad (7)$$

Knowing the non-dimensional number a , the root is obtained immediately.

Frictional fluid

One simple yet effective model is the frictional fluid, especially in the case of coupled behaviour between soil skeleton and pore fluid, but without further additional data it does not allow to obtain the velocity distribution. This is why depth-integrated models using pure frictional models cannot include information concerning depth-integrated stresses $\bar{\sigma}$. Concerning the basal friction, it is usually approximated as

$$\tau_b = -\sigma_v \tan \phi \frac{\bar{v}}{|\bar{v}|} \tag{8}$$

where σ_v is the normal stress acting on the bottom. Sometimes, when there is high mobility of granular particles and drag forces due to the contact with the air are important, it is convenient to introduce the extra term proposed by Voellmy (1955), which includes the correction term $\frac{\rho g v^2}{\xi}$, where ξ is the Voellmy turbulence parameter. Voellmy’s model was initially developed for snow avalanches, and later, Körner (1976) proposed to extend its application range to rock avalanches. Hungr and Evans (1996) provide interesting information regarding modelling of rock avalanches with Voellmy’s model, finding friction coefficients ranging from 0.03 to 0.24, and turbulence coefficients from 100 to 1,000 m/s².

In case the fluidized soil flows over a basal surface made of a different material, if the friction angle between the two materials δ is smaller than the friction angle of the fluidized soil, the basal shear stress is given by:

$$\tau_b = -\rho'_d g h \tan \phi_b \frac{\bar{v}_i}{|\bar{v}|} \tag{9}$$

where the basal friction angle ϕ_b is

$$\phi_b = \min(\delta, \phi) \tag{10}$$

This simplified model can implement the effect of pore pressure at the basal surface. In this case, the basal shear stress will be:

$$\tau_b = -\left(\sigma'_v \tan \phi_b - p_w^b\right) \frac{\bar{v}_i}{|\bar{v}|} \tag{11}$$

We can see that the effect of pore pressure is similar to decreasing the friction angle. This is the basis of the model proposed by Hutchinson (1986) and developed further by Hungr (1995).

Cohesive-frictional fluids

For the case of a simple shear flow, the cohesive-frictional 3D model proposed by Pastor et al. (2009b) reduces to

$$\begin{aligned} \sigma_{11} &= \sigma_{22} = \sigma_{33} = -p \\ \sigma_{13} &= \sigma_{31} = s + \mu_{CF} \left(\frac{\partial v_1}{\partial x_3} \right)^m \end{aligned} \tag{12}$$

where

$$s = c \cos \varphi + p' \sin \varphi. \tag{13}$$

A particular case of interest is the Herschel–Bulkley fluid ($\varphi=0$, $c=\tau_y$, $m>0$), of which the Bingham fluid is a special case ($m=1$).

For cohesionless granular materials, we will use $c=0$, $m=2$. The basal friction term becomes (Pastor et al. 2009b)

$$\tau_b = \rho'_d g h \cos \theta \tan \varphi + \frac{25}{4} \mu_{CF} \frac{\bar{v}^2}{h^2}$$

as it is also obtained for a Criminale–Ericksen–Filbey fluid in the case of plane shear flow (Norem et al. 1987, 1989) and of similar structure as Voellmy’s:

$$\tau_b = \left\{ \rho'_d g h \cos \theta \tan \varphi + \rho g \frac{\bar{v}^2}{\xi} \right\} \tag{14}$$

where ξ is a material parameter. If we compare both expressions, we can see that both incorporate a quadratic term depending on the averaged velocity.

Above, we have defined for convenience $\rho'_d = \rho'_d - \beta_w \rho_w$, where $\rho'_d = (1-n)\rho'_s$, and the pore pressure in excess to the hydrostatic pressure is written as $\Delta p_w = \beta_w p_w$, ρ_w is the density of water, ρ'_s the intrinsic density of the particles, n the void ratio, and ρ'_d the intrinsic density of the debris flow. Initial distribution of pore pressure and its value at the basal surface are important issues. In our depth-integrated model, we assume that the pore pressure at the basal surface is a fraction β_w of the required to induce liquefaction.

Basal erosion

Basal erosion plays a fundamental role in many landslides. While there exists today a number of empirical formulas providing an estimation of erosion for depth-integrated models (Hungr 1995; Chen et al. 2006; Iverson 2012), there is a lack of sound theories able to relate the properties of the sliding mass and the hydro-mechanical characteristics of the basal surface in a consistent way.

A consistent way of modelling the process has been proposed by Crosta et al. (2008) and the results obtained with an ALE model able to reproduce large displacements of a mass are depicted in Fig. 1. This approach allows both 2D and 3D simulations, with an increase in computational cost by roughly two orders of magnitude over 1D or 2D depth-averaged models. Such calculations will become feasible for a wide range of problems in the foreseeable future, but at present the majority of problems will have to be tackled with depth-averaged models.

Depth-integrated codes typically implement simple erosion laws that lack the consistency of the aforementioned approaches. For instance, we can mention: Hungr’s erosion law (Hungr and Evans 2004), the modified erosion law (Egashira 1993, see also Egashira et al. 2001), the path-controlled erosion (Chen et al. 2006) and the erosion law proposed by Blanc (2008). Heuristic erosion laws cannot provide accurate results but may be acceptable for many simple problems.

1. It is useful to distinguish between erosion-limited (or supply-limited) and entrainment-limited (or transport-limited or supply-unlimited) flows (Carson and Kirkby 1972; Gauer and Issler 2004; Jakob 2005; Hungr et al. 2005)

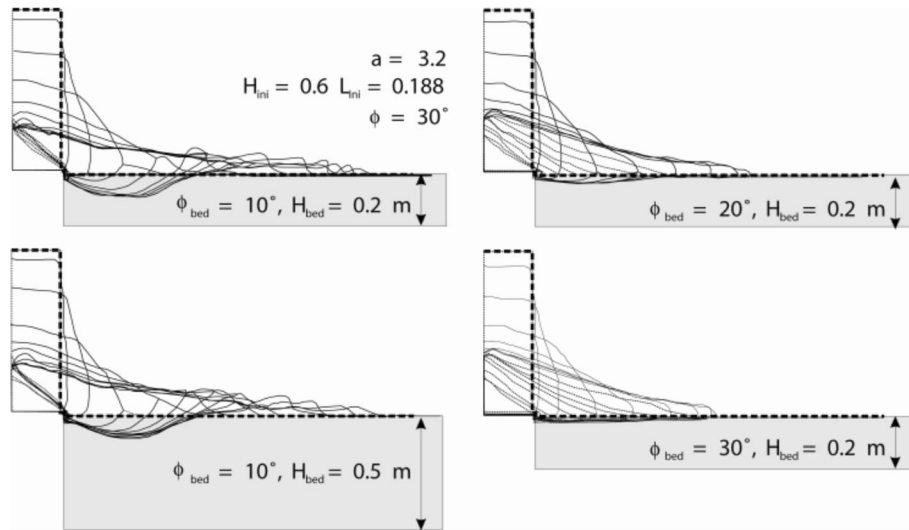


Fig. 1 Results of the numerical models (Crosta et al. 2008) for the 2D collapse of a granular step including the presence of an erodible basal layer (light grey). The layer thickness and internal friction angle have been varied. The time interval between each profile is 0.1 s. The interface between static and moving material is also represented for each instantaneous profile. Low shear strength in the basal layer (left panels) leads to a completely different behaviour of the interface. Deposition is directly simulated without any imposed rule along the interface and the progressive increase of the static sector is observed until the mass comes to rest

In the case of landslides of entrainment-limited type, one expects these models to give erroneous entrainment rates that may substantially affect the run-out distance and deposit distribution. In these cases, we recommend using an entrainment law that is consistent with the flow dynamics. An example is the approach proposed by Issler and Jóhannesson (2011) who determine the dynamically consistent erosion rate of a quasi-stationary flow of Bingham fluid over a brittle bed material without adjustable parameters. Other notable approaches that take into account the acceleration of the eroded material focus on granular materials (Mangeny et al. 2007b) and the effects of pore pressure (Iverson 2012).

In Hungr's erosion law (Hungr 1995), the erosion rate increases in proportion to the flow depth, $dm/ds = E \rho h$, where m is the mass per unit footprint area (units kg m^{-2}), s the distance along the flow path, h the flow depth, and E (units m^{-1}) is a displacement erosion rate, the so-called (spatial) growth rate. This parameter represents the bed-normal depth eroded per unit flow depth and unit longitudinal displacement. It is different from the time-dependent erosion rate e (units m s^{-1}), and is assumed independent of the flow velocity. For example, if E is constant and takes the value

0.01 m^{-1} , the flowing volume increases by 1 % as it travels 1 m. The erosion rate e and the growth rate, E , are related by

$$e = E h \bar{v}, \quad (15)$$

where \bar{v} is the depth-averaged flow velocity (Hungr 1995), and E is an input parameter whose value has to be selected by the user. Hungr's erosion law results in exponential growth of the volume flow with displacement. Although this law is empirical, it has a physical basis in that the stress conditions leading to bed failure and entrainment are related to the total bed-normal stress and thus to the flow depth. Egashira's law is based on flume tests as well as numerical and dimensional analyses. Egashira assumes that the bed slope always adjusts itself to its equilibrium value in case of debris flows travelling over an erodible bed. No consideration is given to pore pressures, even though they can be of paramount importance (this limitation is also inherent to Hungr's model). A more consistent modelling approach of both the flowing mass and the basal materials has been recently proposed by Iverson (2012). Models such as that proposed by Crosta et al. (2009) circumvent the problem in an elegant way considering pore pressure changes associated to volumetric strain and water seepage into the erodible and flowing materials..

Referring to Fig. 2, the mass conservation law can be applied to the yield of eroded material:

$$e_r \Delta_s = e_r v \Delta t = c_* v \Delta h \quad (17)$$

From Eq. (2), in the next step, one obtains

$$\frac{e_r}{v} = c_* \frac{\Delta h}{\Delta_s}$$

Egashira derived the erosion law, substituting the term $\theta - \theta_e = \arctan\left(\frac{\Delta h}{\Delta_s}\right)$ in the last equation:

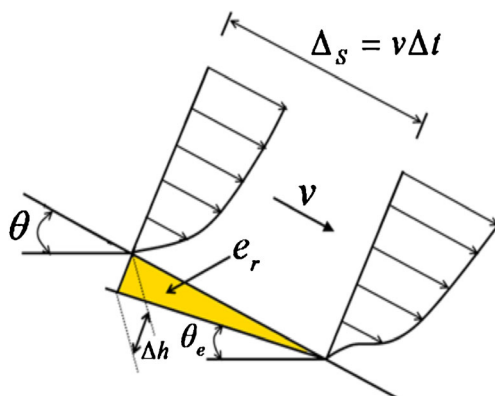


Fig. 2 Sketch depicting the main variables used in Egashira's erosion law

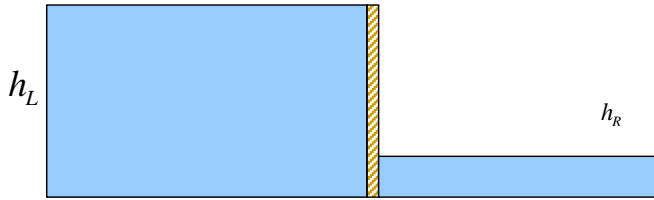


Fig. 3 Dam break over a wet bed

$$e_r = c_* v \tan(\theta - \theta_e) \tag{19}$$

where

- c_* is the bed sediment concentration by volume (of the non-moving layer)
- θ is the bed slope
- θ_e is the equilibrium bed slope, and all the other quantities have been defined previously.

The equilibrium bed slope θ_e is the angle for which the shear strength of the bed surface equals the bed shear stress exerted by a flow. It is assumed that the bed is a cohesionless frictional material and that the debris flow is in dynamic equilibrium. Then, one obtains

$$\theta_e = \tan^{-1} \left\{ \frac{(\sigma - \rho)c}{(\sigma - \rho)c + \rho} \tan \phi \right\}$$

where:

- σ is the mass density of the sediment particles
- ρ the mass density of water
- c the sediment concentration of the debris flow by volume, and
- ϕ the internal bed friction angle, approximated by the basal friction angle ϕ_b . The assumptions made in determining θ_e can, however, be easily modified.

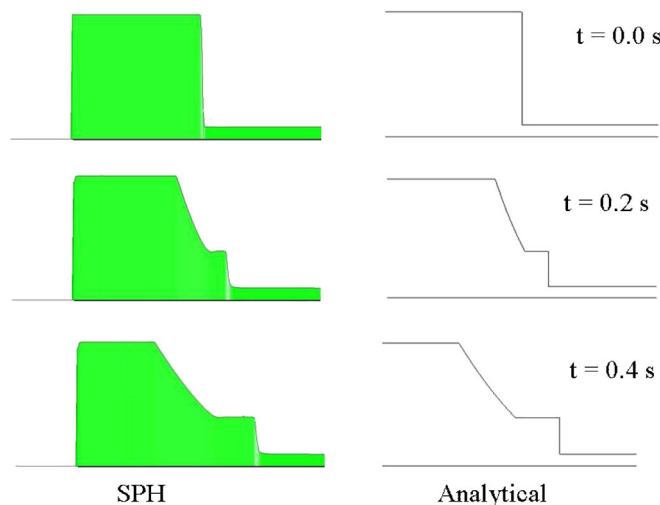


Fig. 4 Computed (left) versus analytical (right) profiles of water depth at 0.0, 0.2 and 0.4 s

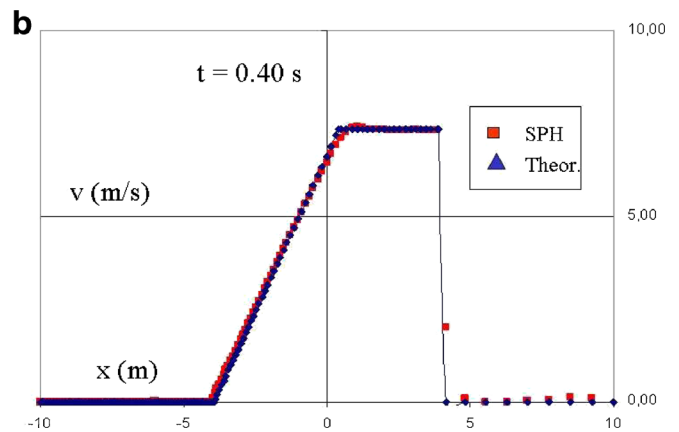
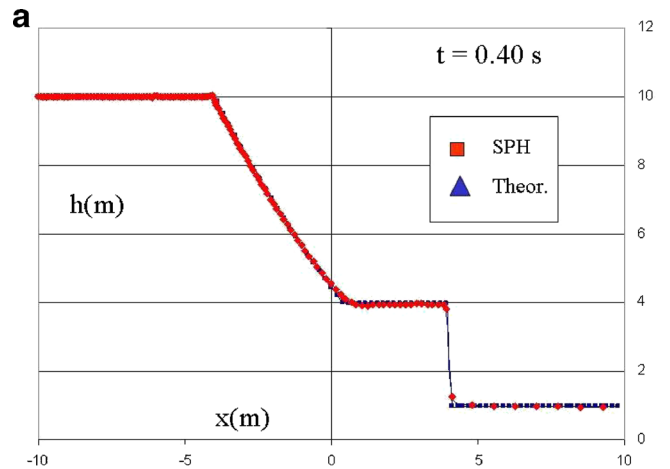


Fig. 5 Wet dam break problem. **a** Comparison between computed and theoretical elevation profiles at time 0.4 s. **b** Comparison between computed and theoretical velocity profiles at time 0.4 s

Experimentally, Takahashi et al. (1992) showed that the sediment concentration of the debris flow (c) does not exceed the value $0.9 c_*$. Therefore, the following condition has to be verified at every timestep:

$$c < 0.9c_*$$

A notable feature of Egashira's model is that it only uses parameters that can either be measured (θ , ϕ , c^* , ρ_p , ρ_w) or are obtained in the course of the calculation (c , v , θ_e).

Implementation of Egashira's erosion law in the 2D SPH depth-integrated model revealed, however, that the erosion

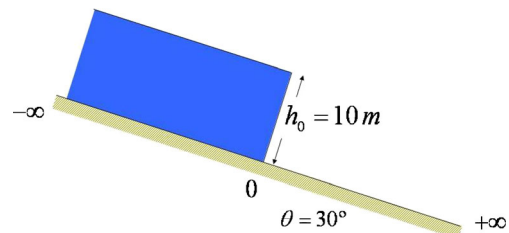


Fig. 6 The frictional dam break problem on an inclined plane

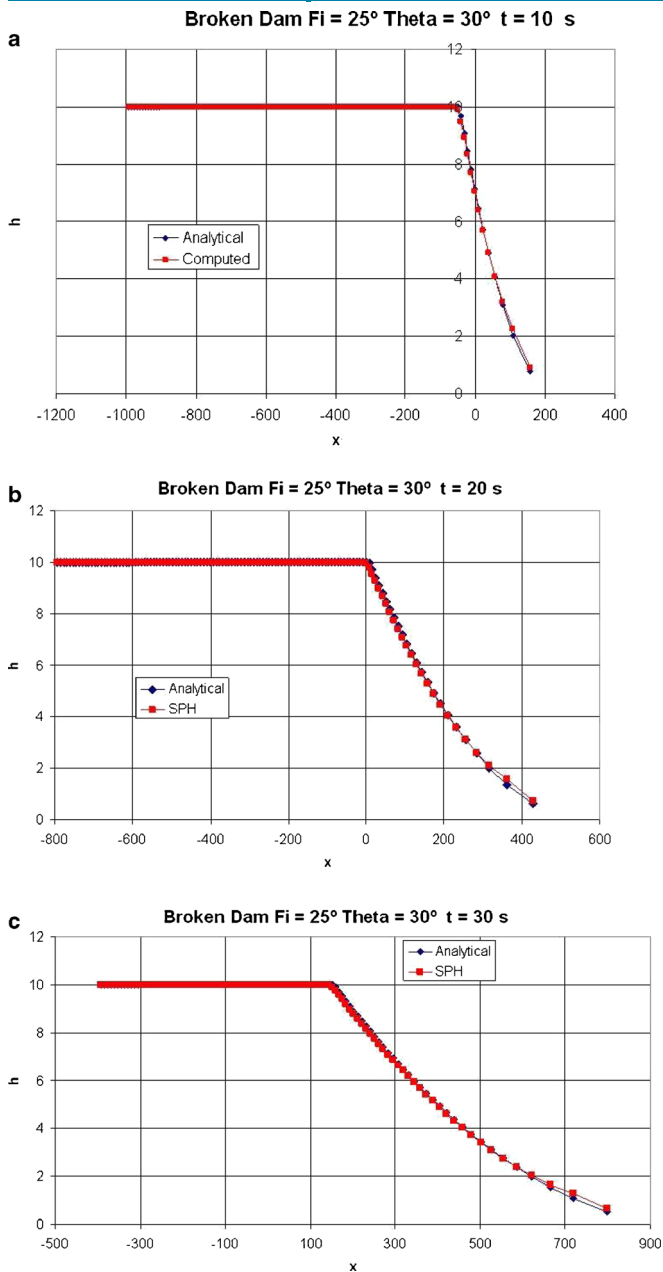


Fig. 7 Dam break problem: **a** $t=10$ s. **b** $t=20$ s. **c** $t=30$ s

rate has to be multiplied by an empirical factor, K , in order to yield realistic results:

$$e_r = Kc_* v \tan(\theta - \theta_e). \quad (21)$$

Blanc's (2008) calibration studies yielded values of K of the order of 10^{-2} , which should be interpreted as indicating that Egashira's basic assumption of proportionality between e_r and $\theta - \theta_e$ fails or that the proposed method for determining the equilibrium slope is not applicable in the case studies, or that the model lacks a consistency constraint from the dynamics of entrainment as opposed to the quasi-static, geotechnical consideration implicit in Eq. (18).

Blanc (2008) proposed a new erosion law combining Egashira's and Hungr's laws, in the form

$$e_r = K \times v \times h \times (\tan\theta)^{2.5} \quad (22)$$

where

K is again an empirical parameter.

This type of equation allows calculating erosion rates by taking into account the slope, flow velocity and flow depth. The proposed equation should be tested by laboratory experiments and validated through case studies. The exponent 2.5 is purely empirical and results from the analysis of a series of experimental data. This law has been introduced in order to represent the variation of the erosion processes taking place during initiation and propagation of the flow and ceasing in the deposition area.

Hungr, Egashira and Blanc laws will be compared later on, in "Influence of topography and erosion law: Tsing Shan debris flow" devoted to Tsing Shan debris flow, where information regarding the erosion that occurred is available.

Numerical model: the SPH approximation

To analyze the propagation of a fast landslide over a complex terrain, the governing partial differential equations have to be discretized for numerical solution in an Eulerian or Lagrangian scheme. The Eulerian schemes are based on a structured (finite differences) or unstructured grid (finite elements and finite volumes) fixed in the space domain and within which the material flows from one cell to another. The main problem lays in the need of a very fine computational mesh for both the terrain and the flow. The Lagrangian methods let the discretization points move along with the flow, allowing the separation of both meshes, with an important economy of computational effort.

Adaptive mesh refinement techniques for fluid problems can be applied to Eulerian methods, as proposed first by Peraire et al. (1987). Since then, adaptivity has been applied to a great variety of problems, including geophysical flows.

However, if we implement the Lagrangian method by means of discretization on a moving mesh, the mesh will rapidly be distorted so severely that frequent remeshing becomes necessary, with a concomitant loss of accuracy and increased computational cost. As an alternative, meshless methods do not rely on meshes for discretization avoiding distortion problems in an elegant way. In this work, we used a meshless method referred to as smoothed particle hydrodynamics (SPH) where information is linked to moving nodes. Adaptivity techniques have also been proposed for meshless methods such as SPH, improving their efficiency very much (Feldman and Bonet 2007).

SPH was introduced independently by Lucy (1977) and Gingold and Monaghan (1977) for astrophysical modelling but it is well suited for hydrodynamics, and a variety of other problems (e.g. Gingold and Monaghan 1982; Monaghan et al. 1999; Bonet and Kulasegaram 2000; Monaghan et al. 2003). SPH has also been applied to model the propagation of catastrophic landslides (Bonet and Rodríguez Paz 2005; McDougall 2006; McDougall and Hungr 2004) but no hydro-mechanical coupling between the solid skeleton and the pore fluid was incorporated in such examples (Pastor et al. 2009a).



Fig. 8 General view of the 2000 Tsing Shan debris flow (left) (King 2001a, b); detail of the bifurcation point (right)

To derive a quasi-Lagrangian formulation of the depth-integrated equations, we first introduce a “quasi-material derivative” as:

$$\frac{\bar{d}}{dt} = \frac{\partial}{\partial t} + \bar{v}_j \frac{\partial}{\partial x_j} \quad j = 1, 2 \quad (23)$$

where \bar{v}_j is the averaged velocity along X_j axis.

From this, we obtain the “quasi-Lagrangian” form of the balance of mass as a depth-integrated equation:

$$\frac{\bar{d}h}{dt} + h \frac{\partial \bar{v}_j}{\partial x_j} = e_R \quad (24)$$

where e_R is the erosion rate [LT^{-1}] and h is the flow depth.

The balance of momentum equation is

$$h \frac{\bar{d}}{dt} \bar{v}_i - \frac{\partial}{\partial x_i} \left(\frac{1}{2} b_3 h^2 \right) = \frac{1}{\rho} \frac{\partial}{\partial x_j} \left(h \bar{\sigma}_{ij}^* \right) + b_i h + \frac{1}{\rho} |N^B| t_i^B - e_R \bar{v}_i \quad (25)$$

where we have introduced the decomposition

$$\sigma_{ij} = -\bar{p} \delta_{ij} + \sigma_{ij}^*$$

with $\bar{p} = \frac{1}{2} \rho b_3 h$ and $\bar{\sigma}_{ij}^* = \sigma_{ij}^* + \bar{p} \delta_{ij}$.

The term t_i^B is the i th component of the normal stress acting on the basal surface, and $|N^B|$ is

$$|N^B| = \left(\frac{\partial Z^2}{\partial x_1} + \frac{\partial Z^2}{\partial x_2} + 1 \right)^{1/2} \quad (26)$$

where Z is the elevation of the basal surface.

We include the effect of centripetal accelerations by integrating the balance of momentum equation along depth, and assuming a constant vertical acceleration given by \bar{v}^2/R , where \bar{v} is the modulus of the averaged velocity, and R the main radius of curvature in the direction of the flow. This simple approach has been shown by the authors (Quecedo and Pastor 2003; Pastor et al. 2008) to provide similar results than those obtained with more consistent formulations using natural coordinate systems (Gray et al. 1999; Savage and Hutter 1989, 1991)

An SPH method for depth-integrated equations

To solve the depth-integrated equations we introduce a set of nodes $\{x_K\}$ with $K=1, \dots, N$ and the nodal variables:

- h_I landslide depth at node I
- \bar{v}_I Depth-averaged 2D velocity
- t_I^b Surface force vector at the flow base
- $\bar{\sigma}_I^*$ Depth-averaged modified stress tensor
- P_{I1} Pore pressure at the basal surface

If the 2D area associated to node I is Ω_I , we will introduce, for convenience, a fictitious mass m_I moving with this node, $m_I = \Omega_I h_I$ and an averaged pressure term \bar{p}_I , given by $\bar{p}_I = \frac{1}{2} b_3 h_I^2$ where b_3 is the component of the gravity acceleration along X_3 .

It is important to note that m_I has no physical meaning, as when node I moves, the material contained in a column of base Ω_I has entered it or will leave it as the column moves with an averaged velocity, which is not the same for all particles in it.

A key ingredient in the meshless discretization of SPH schemes is the notion of a kernel function with compact support, $W(\mathbf{x}, \mathbf{x}')$ that describes how the values of the flow variables at a given point (not generally a node) depend on the values of the flow variables at the nearest nodes \mathbf{x}_j . For example, the flow height at a point \mathbf{x}_I (not a node point in general) can be interpolated from the flow height at the nearest nodes \mathbf{x}_j using the following expression:

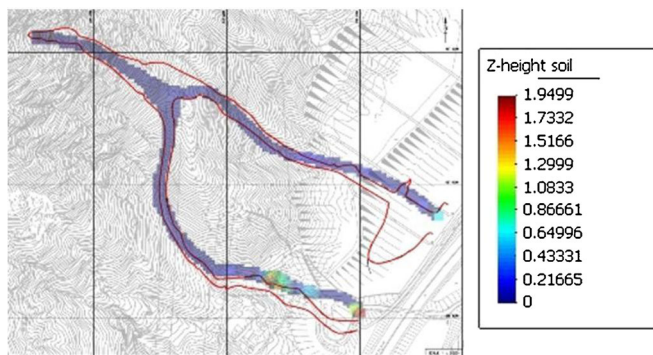


Fig. 9 Tsing Shan debris flow: model predictions vs. field observations with a DTM cell size of 5 m x 5 m

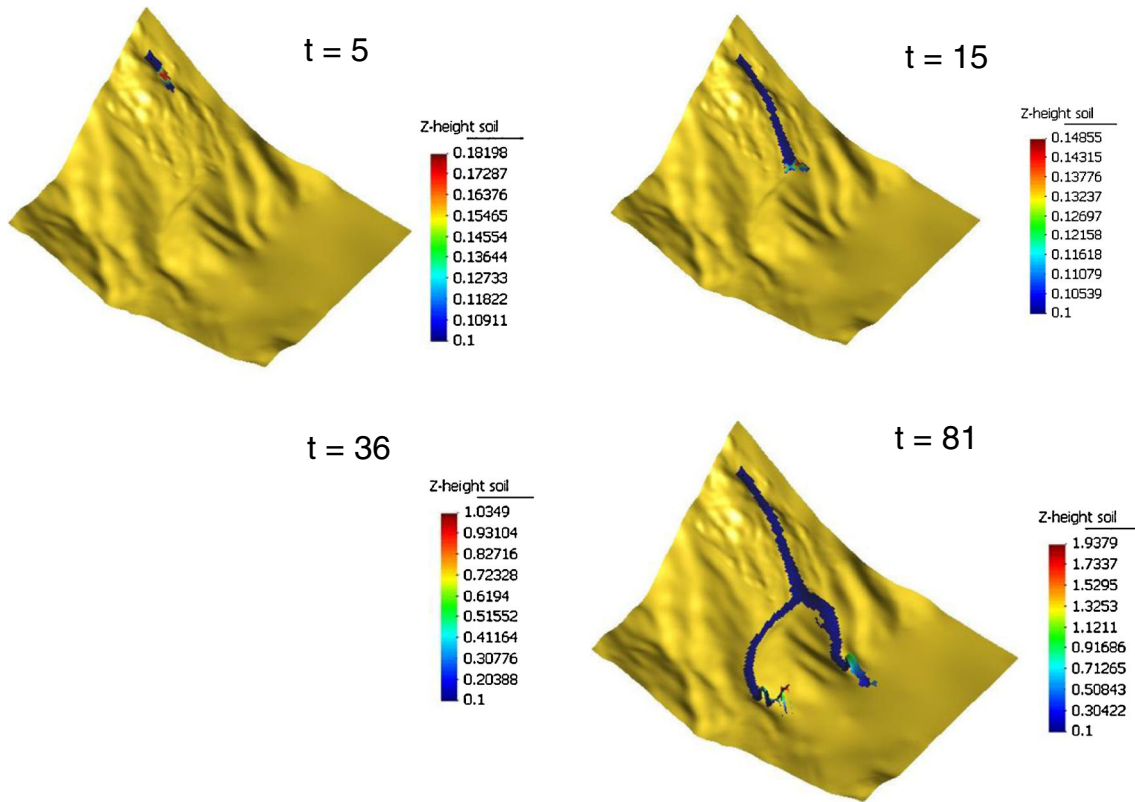


Fig. 10 Tsing Shan debris flow: model predictions at different times with a DTM cell size of $5\text{ m} \times 5\text{ m}$

$$h_I = \langle h(x_I) \rangle = \sum_J h_J \Omega_J W_{IJ} = \sum_J m_J W_{IJ} \quad (27)$$

Here, the notation W_{IJ} is used for $W(\mathbf{x}_I, \mathbf{x}_J) \equiv W(\mathbf{x}_I - \mathbf{x}_J)$. This formulation allows expressing spatial derivatives of the fields through gradients of the kernel function with respect to the node locations. There is some freedom in choosing the kernel function W and in expressing the action of the gradient operator. We will show those obtained with the so-called third symmetrized forms:

$$\frac{\bar{d}h_I}{dt} = h_I \sum_J \frac{m_J}{h_J} v_{IJ} \text{grad } W_{IJ}, \quad (28)$$

where we have introduced $v_{IJ} = v_I - v_J$. The discretized balance of linear momentum equation is:

$$\begin{aligned} \frac{\bar{d}}{dt} \bar{v}_I = & - \sum_J m_J \left(\frac{p_I}{h_I^2} + \frac{p_J}{h_J^2} \right) \text{grad } W_{IJ} \\ & + \frac{1}{\rho} \sum_J m_J \left(\frac{\sigma_I}{h_I^2} + \frac{\sigma_J}{h_J^2} \right) \text{grad } W_{IJ} + b + \frac{1}{\rho h_I} |N^B| t_I^B \end{aligned} \quad (29)$$

Finally, the SPH discretized form of the basal pore pressure P_{1I} dissipation is:

$$\frac{\bar{d}}{dt} P_{1I} = - \frac{\pi^2 c_v}{4h_I} P_{1I} \quad (30)$$

This equation comes from the discretization of a consolidation equation along depth. The pore water pressure profiles are

described by a simple shape function: a quarter cosine profile fulfilling the boundary conditions of zero pore pressure at the surface and zero flux at the bottom. This approach has been used by researchers in the past within the framework of finite element or volumes techniques (Iverson and Denlinger 2001; Pastor et al. 2002, George and Iverson 2011).

Here, the model is simpler, as in Lagrangian formulations convective terms do not appear. The consolidation equation is associated to SPH nodes in our case.

So far, we have discretized the equations of balance of mass, balance of momentum and pore pressure dissipation in space. The resulting equations are ordinary differential equations in time, which can be integrated using a scheme like Leap Frog or Runge–Kutta (second or fourth order).

Examples and applications

The presented depth-integrated SPH model can be used to predict some important features of run-out. In the following, some selected applications to well-described events are presented with parameters selected from back analysis.

First of all, it is important to show how the model is able to reproduce cases for which an analytical solution exists. We have selected the problem of the breaking of a dam over horizontal terrain that is already flooded (wet). This case shows how the proposed model is able to capture shocks, as the solution consists of a rarefaction wave and a shock wave.

A second test will consist on comparing its predictions against a laboratory test. Here, we will use data from a granular avalanche.

Influence of topo mesh $h=2*h_0$

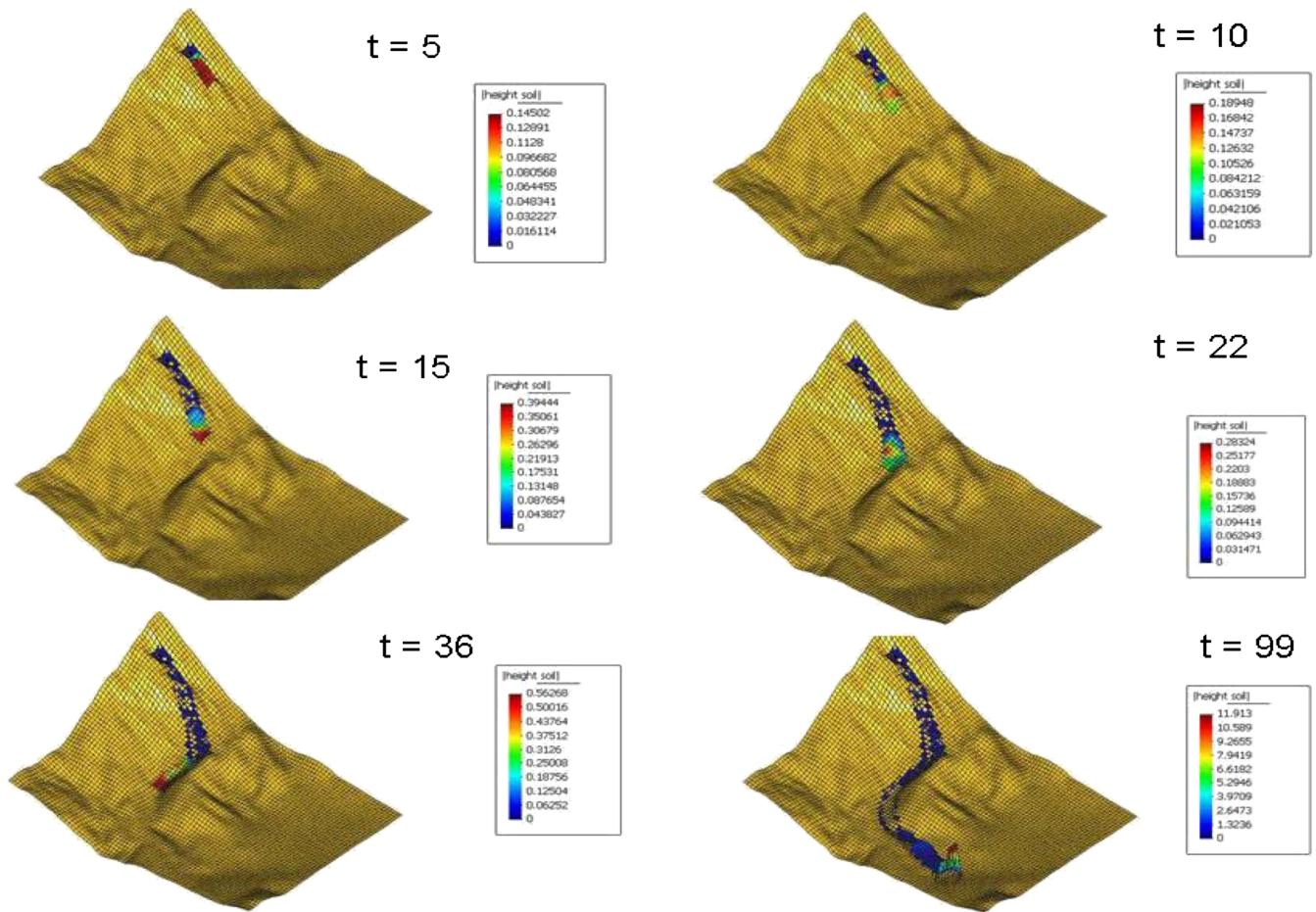


Fig. 11 Tsing Shan debris flow: SPH modelling results obtained by applying a $10\text{ m} \times 10\text{ m}$ DTM cell size. Unrealistic predictions can be compared to those in Figs. 10 and with field observations (Fig. 9)

Finally, we will present some cases for which detailed information has been provided, comparing model predictions against field observations. Field observations have been either obtained from the literature or direct observations.

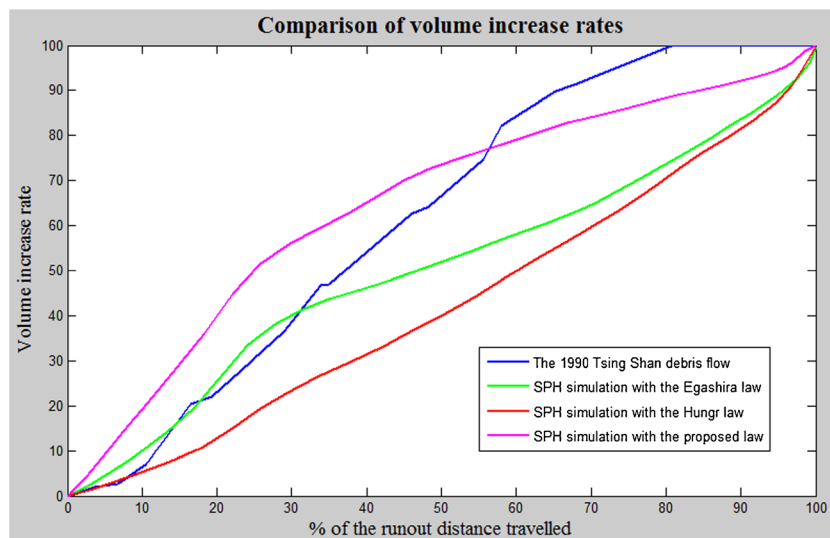


Fig. 12 Comparison of the erosion distribution along the flow path as calculated by different equations for the 1990 Tsing Shan debris flow (after Blanc 2008)

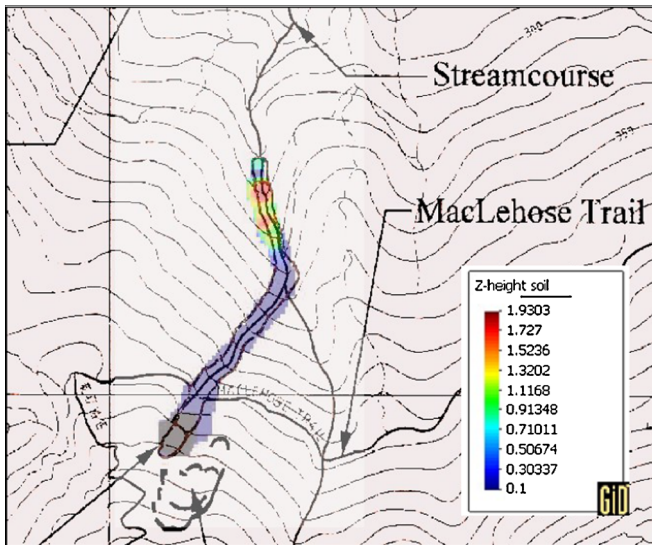


Fig. 13 Model predictions vs field observations for the 2005 event at Tate's Cairn (Hong Kong) by adopting a Voellmy rheology

Pore pressure dissipation has only been taken into account for the Cougar Hill flowslide, because it was reported that soil behaviour showed liquefaction, and the consolidation properties were provided.

Wet dam break model

The test consists of an infinite reservoir of constant depth h_L separated by a vertical wall from a plane flooded with water of depth h_R (Fig. 3). At time $t=0$ the wall is removed instantaneously, and the reservoir water enters the wet plane. The solution (Marshall and Méndez 1981; Toro 2001, and Guinot 2003) consists on a rarefaction wave propagating leftwards, and a shock moving to the right.

Figures 4 and 5 provide a comparison between the analytical solution and the model predictions. Profiles of water depth are given at 0, 0.2 and 0.4 s, and show how the shock is accurately captured.

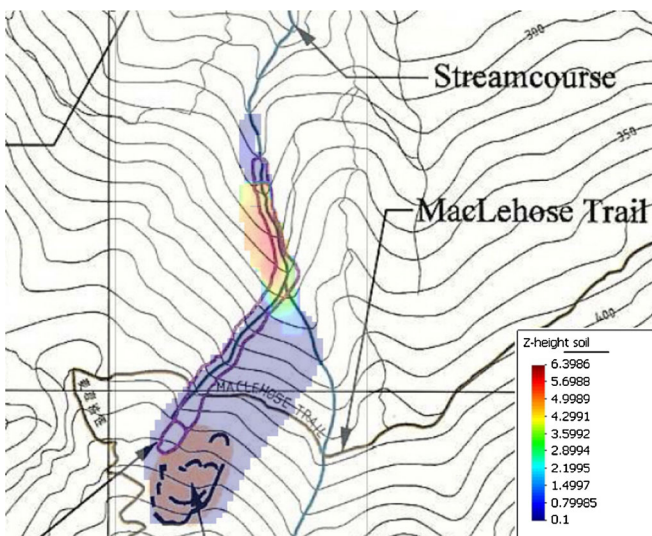


Fig. 14 Model results for Tate's Cairn forwards prediction considering a release of the entire disrupted mass along the slope. Invasion area and final depth are reported

Dambreak problem of a frictional fluid over a slope

In the previous example, we have analyzed the case of a inviscid fluid. It provides information on how the numerical scheme is able to model rarefaction and shock waves. We will consider here the case of a reservoir of a frictional fluid behind a dam on a slope. In this problem, there exist two additional terms (sources), originated by the slope and the friction.

We have used the solution which was proposed by Mangeney et al. 2000. Using the main variables sketched in Fig. 6, the analytical solution is given by:

$$h(t) = \begin{cases} h_0 & x \leq x_L \\ \frac{1}{9g \cos \theta} \left(2c_0 - \frac{x}{t} - \frac{1}{2} mt \right)^2 & x_L \leq x \leq x_R \\ 0 & x_R \leq x \end{cases}$$

The results obtained at times 10, 20 and 30 s are plotted below in Fig. 7a, b, c, showing a good general agreement between theory and computed results.

Influence of topography and erosion law: Tsing Shan debris flow

(a) Model results

The Tsing Shan debris flow occurred in Hong Kong on April 14th, 2000 (King 2001a, b) following heavy rains (160 mm) that triggered more than 50 landslides in the area. The terrain was vegetated, and consisted of colluvial material and boulders. Two features characterize this debris flow event: entrainment along the path causing an increase in volume from 150 to 1,600 m³, and the sharp bifurcation of the flow (see Fig. 8, King 2001a, b).

The fluidized soil is considered to be a viscoplastic frictional fluid with a basal friction given by Eq. (13), where we have used a friction coefficient $\tan \phi = 0.18$ and $\mu_{CF} = 0.00133 \text{ Pa s}^2$.

We have not used the coupled formulation in this case, as no data regarding neither initial distribution of pore pressures nor consolidation properties were provided in the report. We acknowledge it as a limitation of the analysis done, remarking the necessity to obtain laboratory data.

For modelling of erosion (see Basal erosion) we have chosen Hungr's equation by setting the erosion coefficient to 0.0082 m⁻¹.

The debris flow path computed using a 5 m × 5 m DTM cell size, is depicted in Figs. 9 and 10 and shows the branching and the deepest deposit (1.8 m) at the end of the lower south branch. The model predicts a time of propagation close to 120 s and by considering a run-out of 900 m along the lowest branch, the average velocity is close to 30 km/h, but no direct information is available for model calibration. King (2001a, b) states that the total volume deposited in the south branch amounts to 500 m³ with an eroded volume of 1,600 m³, while the computation provides values of 525 m³ and 1,550 m³, respectively.

(b) Influence of terrain representation

In order to illustrate the effect of the DTM size, we ran a simulation by keeping all parameters the same but with a 10 m DTM grid spacing.

The results (Fig. 11) show how the model in this new setting predicts only one branch, instead of the two branches observed

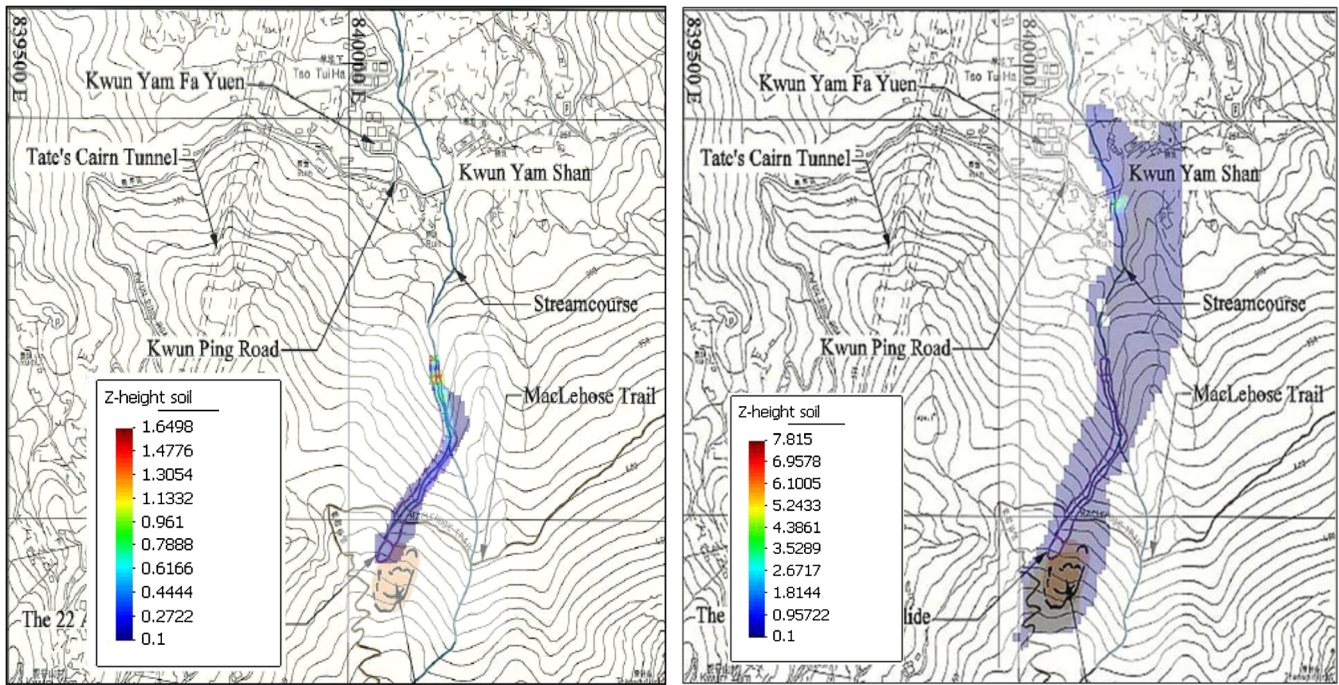


Fig. 15 Model predictions for Tate's Cairn: results obtained with a cohesive fluid model (Bingham) for the two initial masses, a $1,200 \text{ m}^3$ and b $10,000 \text{ m}^3$. These should be compared with results obtained by adopting a Voellmy rheology and reported in Figs. 13 and 14

in reality. We believe that there exist in this case several scales in the topography, which are captured by DTMs with a resolution higher than a threshold. In this case, the 10 m DTM was able to avoid avulsing the debris flow from the channels, but the details causing divergence were smoothed.

A similar analysis for different case studies of volcanic rock-debris avalanches has been performed by Sosio et al. (2011) using ASTER and SRTM topographic data. These authors observed that back analyses performed on different topographic data result in slightly different deposition area and thickness, lateral extent, and flow velocities particularly in case of

unconfined path conditions. Therefore, the calibrated parameters will vary with the adopted topographic data resulting in lower values of the rheological parameters for smaller cell sizes (i.e. larger roughness).

(c) Influence of the erosion law

The influence of the eroded mass depends on the erosion law adopted in the analyses. We depict in Fig. 12 the results obtained with different erosion laws for the Tsing Shan event. In all the calculations with Hungr's erosion equation, the volume increases rapidly in the very last part of the path, which corresponds to the deposition area where no erosion takes place in

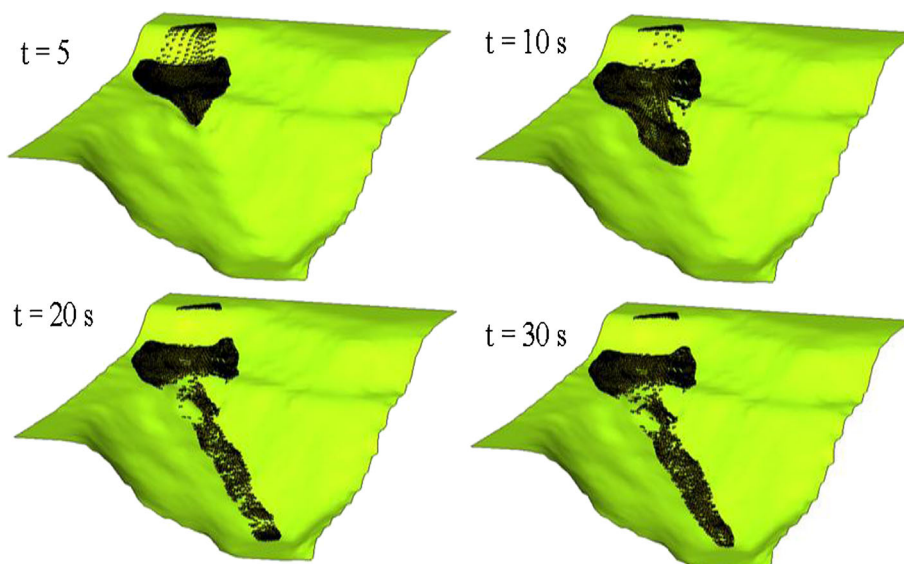


Fig. 16 Cougar Hill: Cougar dump 7 failure. Position of SPH nodes at 5, 10, 20 and 30 s

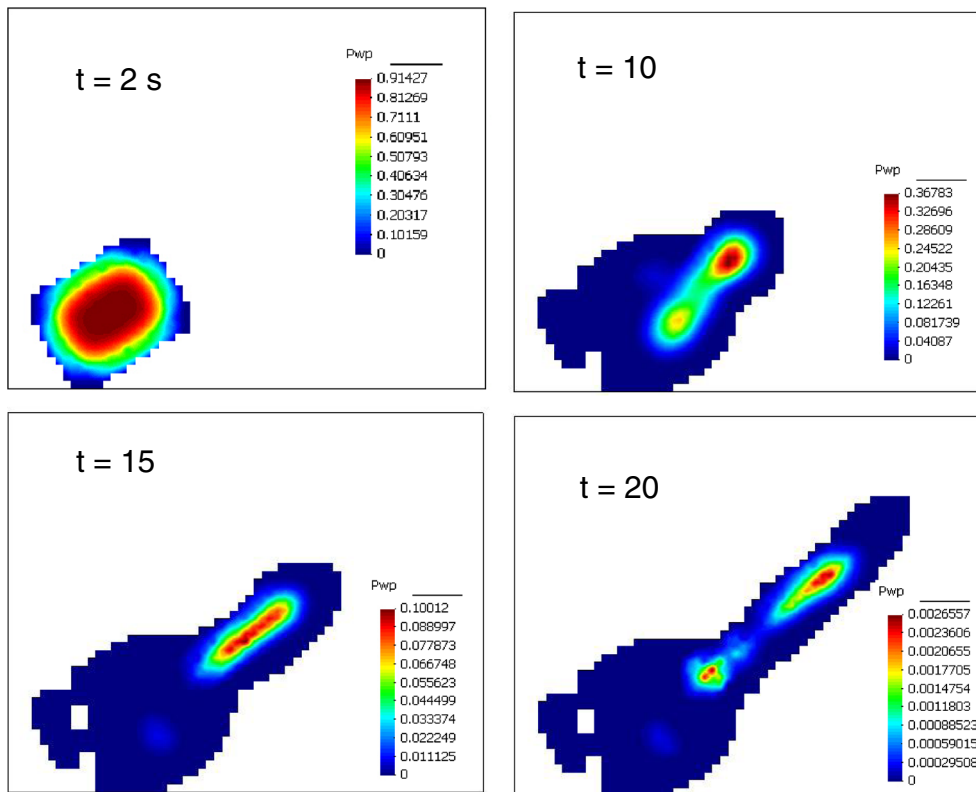


Fig. 17 Cougar Hill: Cougar dump 7 failure Contours of normalized pore water pressure at different time steps. At $t=30$ s. all pore pressures are zero

reality (cf. the 1990 and 2000 Tsing Chan debris flow). Thus while Hungr's equation is able to predict the final volume well, it is unable to evaluate correctly the volume and its changes along the flow path.

The modified Blanc's erosion law provides better results because with these equations most of the debris is accumulated before reaching the deposition area. As a consequence, the erosion occurs mainly during the initiation and the propagation phase.

In case of the 1990 Tsing Chan debris flow, the equation proposed by Blanc (2008) performs best, simulating a greater increase in volume along the initial 50 % of the flow path, and then a further increase at a lower rate.

It is important to notice that choosing a constant value of the erosion constant is a crude approximation, as the areas over which the avalanche travels may consist of different materials.

A forward prediction exercise: The Tate's Cairn debris flow

After a debris flow occurred in Tate's Cairn (Hong Kong), on August 2005 a detailed analysis of the debris source revealed the existence of a disrupted slope, from which more severe events could originate in the future. Starting from the data of the 2005 event (Maunsell Geotechnical Services Ltd. 2007) a simulation has been performed to predict the consequences of a possible debris flow involving the whole disrupted mass A 5 m×5 m DTM provided by the Hong Kong Geotechnical Engineering Office has been used for the simulations. The source area of the 2005 event was 36 m long and 22 m wide with a maximum depth of approximately 5.5 m. The source material consisted of an upper layer of boulder-rich colluvium (or young colluvium) made of slightly sandy silty clay, about 2.9 m thick, and an old colluvium layer made of sandy clayey silt.

A frictional Voellmy-type rheology was chosen and calibration resulted in a turbulence constant $\xi=500$ m/s² and $\tan\phi=0.3$. Hungr's erosion model, with an erosion constant of 0.0006 m⁻¹, was used. The results are given in Fig. 13 and compared with field observations.

Once the past event was modelled, we proceeded to analyze the characteristics of an event affecting the whole presently distressed

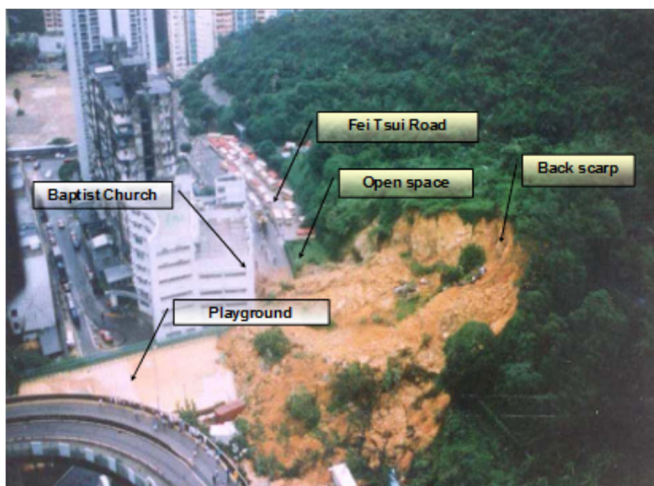


Fig. 18 General view of Fei Tsui Road landslide (Knill and Geotechnical Engineering Office 2006)

Table 1 Parameters used to model Fei Tsui landslide

Fei Tsui Landslide	
Density	19 kN/m ³
Erosion factor	No erosion
Drainage condition	Undrained behaviour
Rheological model	Frictional fluid
Friction angle (apparent)	26°

area. Figure 14 provides the results of the forward prediction, assuming that the same material parameters are representative of fluidized soil behaviour and the same erodible layer thickness will be available.

It is important to note that the reason of using two different rheologies comes from the fact that in some cases, different authors have used different rheological laws to model the same problem. This has happened with Aberfan, where both Bingham and frictional fluids have been used (Jeyapalan et al. 1983; Pastor et al. 2004). However, if one deepens in the literature, finds that the material was loose and metastable, with tendency to liquefy. Hence, it is more logical to use a frictional model than a Bingham rheology.

Influence of the rheological model

The choice of a different rheological model to back analyse an event can still succeed in fitting the final deposit but this choice will also control the final result and prediction performance of the model. As a consequence, a correct choice of the model rheology should be based on the type of phenomenon and field observations of past events. In the following we demonstrate what occurs in case of the Tate's Cairn case study when a Bingham rheology is used to calibrate against the past event and the obtained calibrated values are used for a forward run-out prediction.

By calibrating the model with a Bingham fluid rheology, a yield stress of 2,860 Pa and viscosity coefficient of 44.8 Pa s were found. The results for the backward and forward predictions are given in

Fig. 15 where it is possible to observe a much different behaviour of the two forward predictions with respect to the results reported in Figs. 13 and 14.

This example stresses the point that fitting a model to a set of observations is not enough. Given the type of phenomenon, it is not reasonable to use a Bingham model in this case, but this rheology is able to provide good results for that particular mass of soil and the initial volume.

Influence of basal pore water pressure: Cougar Hill flowslide

It has been already stated that the coupling between pore pressures and the solid skeleton is crucial for many flowslides and should be included in modelling their propagation. Dawson et al. (1998) reported three cases of flowslides in a coal mine waste dump in the Western Canadian Rocky Mountains, selected among some 50 flowslides that occurred between 1972 and 1997. The flowslides propagated distances up to 3,500 m, with a mean value of 980 m and with run-out distances exceeding 1,000 m in case of rapid loading of saturated materials along the distal run-out path.

In the case of the Cougar 7 dump failure in May 1992, approximately 200,000 m³ slid off the 100 m high dump. Wet fine-grained layers were found at the foundation contact, near the crest, and in the debris. According to Dawson et al., these fine-grained layers played a crucial role in both the initiation and the propagation phases. The flowslide is thought to have been triggered by liquefaction of the fine-grained layers. Laboratory tests gave a density of 1,900 kg m⁻³, an effective friction angle $\phi' = 37^\circ$ and a characteristic consolidation time of 68 s, from which a value of $c_v = 1.76 \cdot 10^{-3} \text{ m}^2 \text{ s}^{-1}$ was derived. The initial pore pressure was assumed to be 0.89 times the value required to reach full liquefaction, whereas the value of the effective friction angle was taken directly from experiments by Dawson et al. (1998) even if a smaller friction angle could have provided good predictions.

The results of the simulations are given in Figs. 16 and 17, in terms of the flowslide extent, debris depth and pore pressures.

The pore pressure distribution follows and controls at the same time the evolution of the flow, remaining high in the central part of

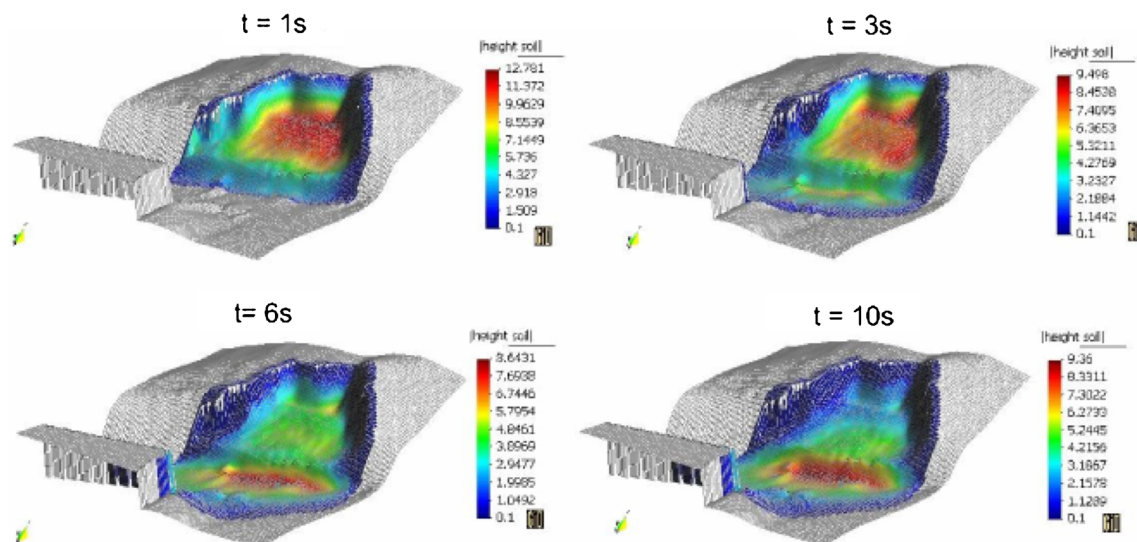


Fig. 19 SPH model results showing the Fei Tsui Road landslide (Hong Kong) propagation at four time steps

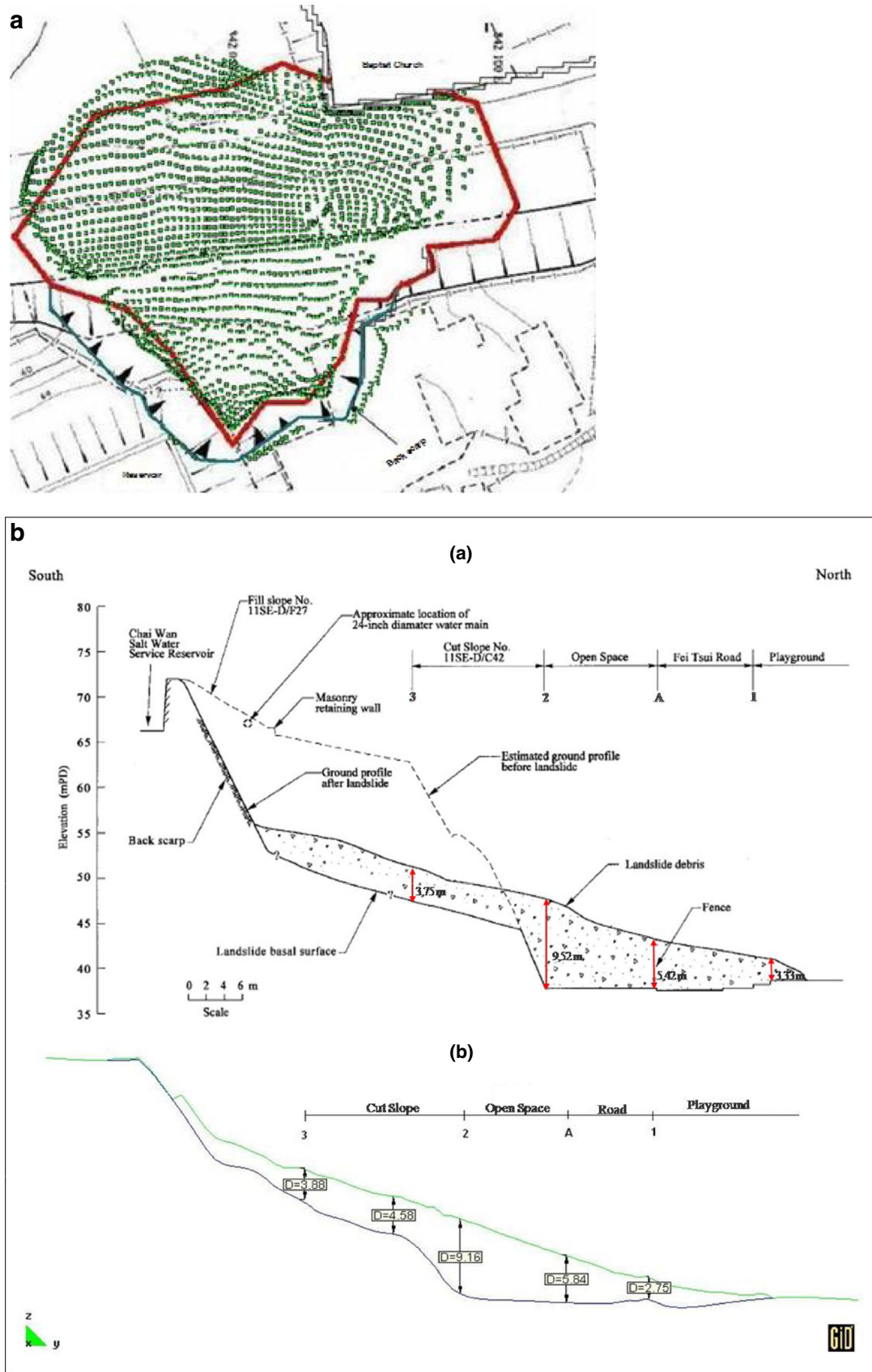


Fig. 20 a Fei Tsui Road landslide (Hong Kong): comparison between the extent of the real landslide and the SPH modelling results. b Comparison between vertical profiles A–A': (top) field measurements and (bottom) computed results

Table 2 Values for the actual debris deposits and model

	Landslide (m)	Modelling (m)	Difference (%)
Maximum width of the debris deposit	90	88.70	-1.44
Maximum horizontal distance	70	82.60	+18.00
Depth on point 2, profile A-A'	9.52	9.16	-3.78
Depth on point 3, profile A-A'	3.75	3.88	+3.47
Depth on point A, profile A-A'	5.42	5.84	+7.75
Depth on point 1, profile A-A'	3.33	2.75	-17.41
Maximum depth of debris piled against the corner of the church (point P)	6	5.20	+13.3

the flow and rapidly decreasing towards the flow boundary (both laterally and toward the front). This reasonably reflects the experimental observations.

Short run-out rockslide-avalanche: Fei Tsui Road landslide

The Fei Tsui Road (Knill and Geotechnical Engineering Office 2006), occurred on August 2005 on a 60° slope in weathered volcanic rock, grading from moderately to completely decomposed tuff. It involved 14,000 m³ of material with two groundwater systems, the regional groundwater table and a perched water table. The causes are described as a combination of a weak material together with the groundwater recharge following a prolonged heavy rainfall. The maximum width of the mobilized mass was 90 m, and the distance travelled 70 m, after which the landslide piled some 6 m up against a corner of the Baptist Church building. Figure 18 (Knill and Geotechnical Engineering 2006) shows a general view of the landslide. Because of the high thickness to length ratio, the applicability of depth-integrated models to this landslide is questionable.

The landslide has been modelled using a frictional fluid with an internal friction angle of 26° (Knill and Geotechnical Engineering 2006) representing an apparent friction angle smaller than the effective friction angle in presence of induced pore pressures. Taking into account the time of propagation (about 10 s) and the involved mass, it has been assumed that the time of propagation is much smaller than the time required for pore pressure dissipation, inducing a condition of undrained loading. Table 1 summarizes the parameters used.

Figure 19 depicts the position of the landslide at successive times (1, 3, 6, and 9 s), and Fig. 20a, b shows comparison of computed results and measurements both for the run-out and the vertical profile A-A', with site measurements and model predictions at specific points.

We have evaluated the precision of the results by comparing the values in the model with field measurements. As references, we have chosen the run-out, the dimensions of the debris deposit and the thickness of the material deposited at some points of the profile A-A', and the corner of the church (point P).

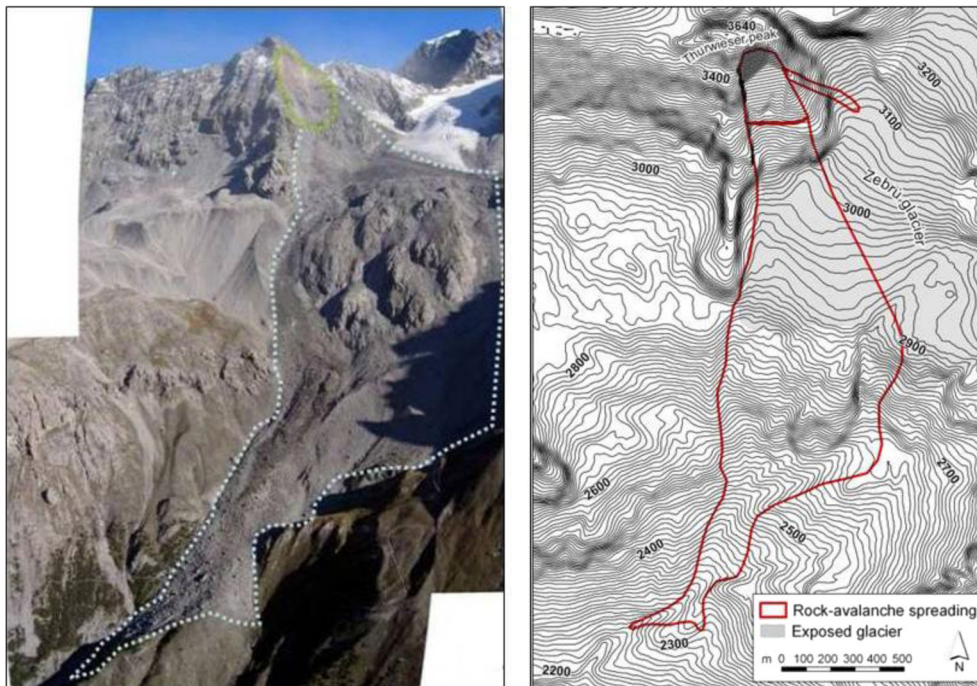


Fig. 21 General view of Thurwieser rock avalanche (Sosio et al. 2008) and map with of the source, transport and deposition

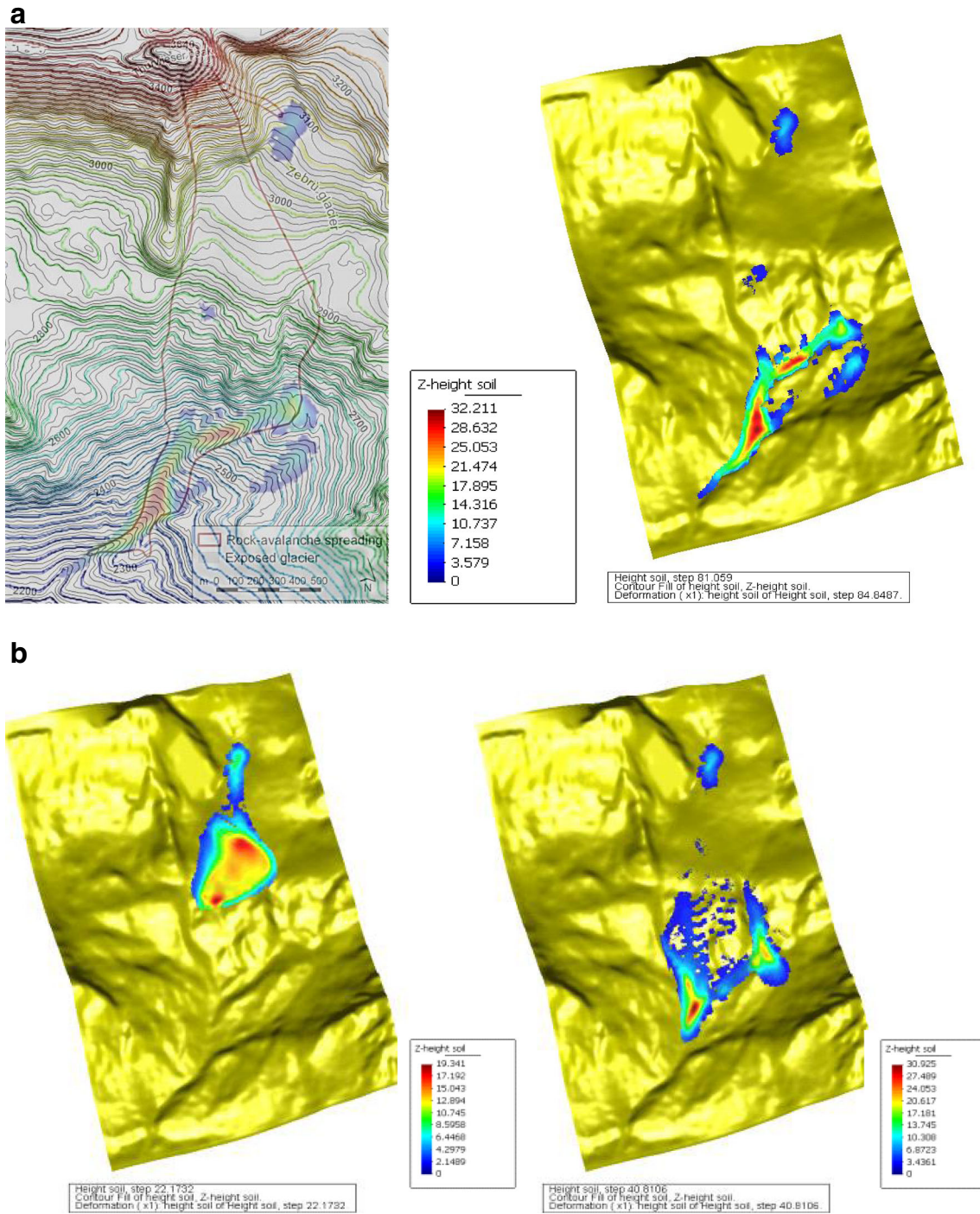


Fig. 22 a Thurwieser avalanche final extension after 81 s: computed results (*colorful isolines* and deposit height) versus field measurements (*black isolines* and *red line* for the spreading). b Thurwieser avalanche extension after 22 and 40 s with deposit height

The agreement for the depth and the maximum width of the deposit was excellent, and the result for the run-out was good enough. However, the maximum distance travelled was overestimated by 18 %. Table 2 contains the actual values, the program's results and the differences expressed as percentages.

Run-out on different materials: Thurwieser rock avalanche

The $2.2 \times 10^6 \text{ m}^3$ Thurwieser rock avalanche occurred in the Central Italian Alps on 18th September 2004 detaching from a steep rock

face, and propagating from 3,500 to 2,300 m of altitude, with a travel distance of 2.9 km. Sosio et al. (2008) describe all the phases of this avalanche providing detailed information concerning the avalanche velocity during the entire evolution (Fig. 21).

This avalanche presents several modelling difficulties represented by the initial steep failure and the crossing of terrains of different materials (e.g. Zebrú glacier). The basal friction along the glacier surface is very small, and erosion of ice and snow is

possible. This entrained material can melt due to the heat generated by basal friction, providing extra water, and probably originating basal pore pressures (Schneider et al. 2011; Sosio et al. 2012). A simple frictional Voellmy model including turbulence has been used with erosion described by Hungr's equation (1995). The calibrated rheological parameters are: $\tan \phi = 0.39$, Voellmy coefficient $1,000 \text{ m/s}^2$, erosion coefficient 0.00025 m^{-1} .

The results are given in Fig. 22, where the avalanche evolution with time and the computed final extent together with field observations are plotted.

In this case—a rock avalanche—no pore water pressure analysis was done. We agree that the problem is quite complex, as rock fragmentation may generate a tendency to compact, resulting on an increase of air pore pressure at the beginning. This mechanism can be balanced by a tendency to dilate because of the shear strain rate (indeed, in rheometers, the granular materials dilate as strain rate increases) Later, when the avalanche is crossing the glacier, because of the friction, melting can result on water entering the avalanching material. We have not included these effects, and consider it as a limitation of the model.

Conclusions

Rock avalanches, flowslides, debris flows, lahars and similar events are very complex phenomena involving a multitude of physical mechanisms such as break-up and comminution, segregation, recirculation basal erosion, coupling with pore water, evolution of fluid properties, and thermal effects. Complete 3D models based on mixture theory and incorporating sub-models for the phenomena mentioned above are still very expensive from a computational point of view. Depth-integrated models provide a good combination of simplification and accuracy. A choice of suitable discretization techniques exists, such as finite differences, finite elements, finite volumes or more recent meshless methods (e.g. SPH). All of them provide accurate numerical approximations of the depth-integrated equations.

The aim of this paper has been to show the potential of depth-integrated, SPH models incorporating pore pressure dissipation to simulate the propagation phase of some types of landslides, describing some of the inaccuracies which can appear in the discretization.

The SPH approach allows to separate the moving nodes or particles, which represent the flow without a mesh, from the topographical mesh, which may be structured (DTM cells) to simplify computations. In the authors' experience, the computational time can be reduced up to 30 times as compared with unstructured finite element meshes.

The cases which have been considered include (i) problems having analytical solution (ii) real events.

In the former group, the SPH model used here provides reasonable results both for shock and rarefaction waves which appear in the case of a dam breaking over a flooded domain, and when a dam impounding a granular fluid breaks on a sloping terrain.

Concerning the real events which have been analyzed, we have considered a rock avalanche, two cases of debris flows, a short run-out landslide and a flowslide where pore pressure dissipation was important.

Calibration has depended on the quality and the amount of available data. Depth-integrated models use relatively few material parameters, which in some cases have to be obtained by back

analysis (trial and error), while in others, friction angle and consolidation properties have been determined by suitable laboratory tests

Concerning the initial mass, the result obviously depends on it, and also on initial pore pressures. This information is crucial for flowslides, but most of the times it is not available, and has to be assumed. This is the case the case of very loose metastable materials, where pore pressures generated in the triggering process largely contribute to failure. Liquefaction is possible also in dry materials under special circumstances, with air playing the role of pore fluid (Fernández-Merodo et al. 2004; Roche et al. 2008). The importance of the pore pressure on propagation depends on the ratio of consolidation and propagation times.

The resolution of the DTM can be determinant in some cases, such as the Tsing Shan debris flow presented here.

Finally, we have to point out the importance of modelling the different properties of the terrain over which the landslide propagates, which can affect basal friction angle (as in the case of Thurwiesser avalanche) and erosion.

Acknowledgments

The authors wish to thank the Geotechnical Engineering Office, Civil Engineering and Development Department of the Government of the Hong Kong SAR for providing the digital terrain models for the Hong Kong landslide cases. The financial support of the Spanish MCINN (Project GeoDyn), and the EC-Project SafeLand (FP7 European project "Living with landslide risk in Europe: Assessment, effects of global change, and risk management strategies") are gratefully acknowledged.

References

- Agliardi F, Crosta GB (2003) High resolution three-dimensional numerical modelling of rockfalls. *Int J Rock Mech Min Sci* 40:455–471
- Alonso EE, Pinyol NM (2010) Criteria for rapid sliding. I: a review of the Vaiont case. *Eng Geol* 114:198–210
- Biot MA (1941) General theory of three-dimensional consolidation. *J Appl Phys* 12:155–164
- Biot MA (1955) Theory of elasticity and consolidation for a porous anisotropic solid. *J Appl Phys* 26:182–185
- Blanc T (2008) Numerical simulation of debris flows with the 2D SPH depth-integrated model. Master's thesis, Institute for Mountain Risk Engineering, University of Natural Resources and Applied Life Sciences, Vienna, Austria
- Bonet J, Kulasegaram S (2000) Correction and stabilization of smooth particle hydrodynamics methods with applications in metal forming simulations. *Int J Numer Methods Eng* 47:1189–1214
- Bonet J, Rodríguez Paz MX (2005) A corrected smooth particle hydrodynamics formulation of the shallow-water equations. *Comput Struct* 83:1396–1410
- Briukhanov AV, Grigorian SS, Miagkov SM, Plam MYa, Shurova IYa, Eglit ME, Yakimov YuL (1967) On some new approaches to the dynamics of snow avalanches. In: Ōura H (ed) *Physics of Snow and Ice*, Proc. Intl. Conf. Low Temperature Science, Sapporo, Japan, 1966. Institute of Low Temperature Science, Hokkaido University, Sapporo, Hokkaido, Japan. Vol. 1, Part 2, pp. 1223–1241
- Calvetti F, Crosta G, Tatarella M (2000) Numerical simulation of dry granular flows: from the reproduction of small-scale experiments to the prediction of rock avalanches. *Riv Ital Geotecnica* 2000:21–38
- Cannon SH (1993) An empirical model for the volume-change behaviour of debris flows. In: Shen HW, Su ST, Wen F (eds) *Proceedings of Hydraulic Engineering'93*, San Francisco. American Society of Civil Engineers, New York, USA. Vol. 2, pp. 1768–1773
- Carson MA, Kirkby MJ (1972) *Hillslope form and process*. Cambridge University Press, Cambridge, pp 13–17, 372–377

- Chen H, Crosta GB, Lee CF (2006) Erosional effects on run-out of fast landslides, debris flows and avalanches: a numerical investigation. *Geotechnique* 56(5):305–322
- Corominas J (1996) The angle of reach as a mobility index for small and large landslides. *Can Geotech J* 33:260–271
- Coussy O (1995) *Mechanics of porous media*. Wiley, Chichester
- Crosta GB, Cucchiari S, Frattini P (2003) Validation of semi-empirical relationships for the definition of debris-flow behaviour in granular materials. In: Rickenmann D, Chen CI (eds) *Debris-flow hazards mitigation: mechanics, prediction and assessment*. Millpress, Rotterdam, pp 821–831
- Crosta GB, Imposimato S, Roddeman DG (2008) Numerical modelling of entrainment/deposition in rock and debris-avalanches. *Eng Geol* 109(1–2):135–145. doi:10.1016/j.enggeo.2008.10.004
- Crosta GB, Imposimato S, Roddeman D (2009) Numerical modeling of 2-D granular step collapse on erodible and nonerodible surface. *J Geophys Res* 114, F03020. doi:10.1029/2008JF001186
- Daouadji A, Hicher P-Y (2010) An enhanced constitutive model for crushable granular materials. *Int J Numer Anal Meth Geomech* 34:555–580. doi:10.1002/nag.815
- Dawson RF, Morgenstern NR, Stokes AW (1998) Liquefaction flowslides in Rocky Mountains coal mine waste dumps. *Can Geotech J* 35:328–343
- de Boer R (2000) *Theory of porous media*. Springer, Berlin
- Egashira S (1993) Mechanism of sediment deposition from debris flow (part 1). *Jpn Soc Erosion Control Eng* 46(1), 186: 45–49 (in Japanese)
- Egashira S, Honda N, Itoh T (2001) Experimental study on the entrainment of bed material into debris flow. *Phys Chem Earth (C)* 26(9):645–650
- Evans SG, Hungr O (1993) The assessment of rockfall hazard at the base of talus slopes. *Can Geotech J* 30:620–636
- Fannin RJ, Wise MP (2001) An empirical-statistical model for debris flow travel distance. *Can Geotech J* 38:982–994
- Feldman J, Bonet J (2007) Dynamic refinement and boundary contact forces in SPH with applications in fluid flow problems. *Int J Num Methods Eng* 72:295–324. doi:10.1002/nme.2010
- Fell R, Corominas J, Bonnard C, Cascini L, Leroi E, Savage WZ (2008) Guidelines for landslide susceptibility, hazard and risk zoning for land use planning. *Jt Tech Comm Landslides Eng Slopes Eng Geol* 102:85–98
- Fernández-Merodo JA, Pastor M, Mira P, Tonni L, Herreros MI, Gonzalez E, Tamagnini R (2004) Modelling of diffuse failure mechanisms of catastrophic landslides. *Comput Methods Appl Mech Eng* 193:2911–2939
- Gauer P, Issler D (2004) Possible erosion mechanisms in snow avalanches. *Ann Glaciol* 38:384–392
- George DL, Iverson RM (2011) A two-phase debris-flow model that includes coupled evolution of volume fractions, granular dilatancy, and pore-fluid pressure. *Ital J Eng Geol Environ*. doi:10.4408/IJEGE.2011-03.B-047
- Gingold RA, Monaghan JJ (1977) Smoothed particle hydrodynamics. *Mon Not R Astron Soc* 181:375–389
- Gingold RA, Monaghan JJ (1982) Kernel estimates as a basis for general particle methods in hydrodynamics. *J Comput Phys* 46:429–453
- Gray JMNT, Ancy C (2011) Multi-component particle-size segregation in shallow granular avalanches. *J Fluid Mech* 678:535–588
- Gray JMNT, Thornton AR (2005) A theory for particle size segregation in shallow granular free-surface flows. *Proc R Soc Math Phys Eng Sci* 461(2057):1447–1473
- Gray JMNT, Wieland M, Hutter K (1999) Gravity-driven free surface flow of granular avalanches over complex basal topography. *Proc R Soc Lond* 455:1841–1874
- Guinot V (2003) *Godunov-type schemes. An Introduction for Engineers*. Elsevier, Amsterdam
- Hu W, Yin ZY, Dano C, Hicher PY (2012) Numerical study of crushable granular materials. In: *Deformation characteristics of Geomaterials: Proceedings of the Fifth International Symposium on Deformation Characteristics of Geomaterials, Is-Seoul 2011, 1–3 September 2011, Seoul, Korea*. IOS Press, p. 404
- Hungr O (1995) A model for the run-out analysis of rapid flow slides, debris flows, and avalanches. *Can Geotech J* 32:610–623
- Hungr O, Evans SG (1988) Engineering evaluation of fragmental rockfall hazards. In: Bonnard (ed), *5th International Symposium on Landslides, Lausanne, Switzerland*. A. A. Balkema, vol. 1, pp. 685–690
- Hungr O, Evans SG (1996) Rock avalanche runout prediction using a dynamic model. In: *Proceedings of the 7th International Symposium on Landslides, Trondheim, Norway, Vol. 17*, p. 21
- Hungr O, Evans SG (2004) Entrainment of debris in rock avalanches: an analysis of a long run-out mechanism. *Geol Soc Am Bull* 116(9/10):1240–1252
- Hungr O, McDougall S, Bovis M (2005) Entrainment of material by debris flows. In: Jakob M, Hungr O (eds) *Debris flow hazard and related phenomena*, chapter 7. Springer and Praxis, Berlin, pp 135–158
- Hunter G, Fell R (2003) Travel distance angle for rapid landslides in constructed and natural slopes. *Can Geotech J* 40:1123–1141
- Hutchinson JN (1986) A sliding-consolidation model for flow slides. *Can Geotech J* 23:115–126
- Issler D, Jóhannesson T (2011) Dynamically consistent entrainment and deposition rates in depth-averaged gravity mass flow models. Norwegian Geotechnical Institute, Oslo, Technical Note 20110112-00-1-TN
- Iverson RM (2012) Elementary theory of bed-sediment entrainment by debris flows and avalanches. *J Geophys Res* 117, F03006. doi:10.1029/2011JF002189, 17 pp
- Iverson RM, Denlinger RP (2001) Flow of variably fluidized granular masses across three dimensional terrain. 1. Coulomb mixture theory. *J Geophys Res* 106(B1):537–552
- Iverson RM, Schilling SP, Vallance JW (1998) Objective delineation of lahar inundation hazard zones. *Geol Soc Am Bull* 110:972–984
- Iverson NR, Mann JE, Iverson RM (2010) Effects of soil aggregates on debris-flow mobilization: results from ring-shear experiments. *Eng Geol* 114(1):84–92
- Jakob M (2005) Debris-flow hazard analysis. In: Jakob M, Hungr O (eds) *Debris flow hazard and related phenomena*, chapter 17. Springer and Praxis, Berlin
- Jeyapalan JK, Duncan JM, Seed HB (1983) Investigation of flow failures of tailing dams. *J Geotech Eng ASCE* 109:172–189
- Johnson CG, Kokelaar BP, Iverson RM, Logan M, LaHusen RG, Gray JMNT (2012) Grain-size segregation and levee formation in geophysical mass flows. *J Geophys Res* 117. doi:10.1029/2011JF002185, 23 p
- Kikumoto M, Muir Wood D, Russell AR (2009) Particle crushing and deformation behaviour. *Int. Symp. on Prediction and Simulation Methods for Geohazard Mitigation (IS-Kyoto)*, Kyoto, Japan, 2010, 50(4):547–563
- King JP (2001a) The Tsing Shan debris flow and debris flood. *Landslide study report LSR 2/2001*, Geotechnical Engineering Office, Civil Engineering and Development Department, The Government of the Hong Kong Special Administrative Region, Hong Kong, People's Republic of China, 216 pages
- King JP (2001b) The 2000 Tsing Shan Debris Flow and Debris Flood. *Landslide study report No. LSR 3/2001*, Geotechnical Engineering Office, Civil Engineering and Development Department, The Government of the Hong Kong Special Administrative Region, Hong Kong, People's Republic of China, 54 pages
- Knill SJ, Geotechnical Engineering Office (2006) Report on the Fei Tsui road landslide of 13 August 1995. *GEO REPORT no. 188*. Geotechnical Engineering Office, Civil Engineering and Development Department, The Government of the Hong Kong Special Administrative Region, Hong Kong, People's Republic of China
- Körner HJ (1976) Reichweite und Geschwindigkeit von Bergstürzen und Fließschneelawinen. *Rock Mech* 8(4):225–256
- Lewis RL, Schrefler BA (1998) *The finite element method in the static and dynamic deformation and consolidation of porous media*. Wiley, Hoboken
- Lied K, Bakkehoi S (1980) Empirical calculations of snow-avalanche run-out distance based on topographic parameters. *J Glaciol* 26:165–177
- Lucy LB (1977) A numerical approach to the testing of fusion process. *Astron J* 82:1013–1024
- Mangeny A, Heirich P, Roche R (2000) Analytical solution for testing debris avalanche numerical models. *Pure Appl Geophys* 157:1081–1096
- Mangeny A, Bouchut F, Thomas N, Vilotte JP, Bristeau MO (2007a) Numerical modeling of self-channeling granular flows and of their levee-channel deposits. *J Geophys Res* 112, F02017. doi:10.1029/2006JF000469
- Mangeny A, Tsimiring LS, Volfson D, Aranson IS, Bouchut F (2007b) Avalanche mobility induced by the presence of an erodible bed and associated entrainment. *Geophys Res Lett* 34, L22401
- Marshall G, Méndez R (1981) Computational aspects of the random choice method for shallow water equations. *J Comput Phys* 39(1):1–21
- Maunsell Geotechnical Services Ltd (2007) Detailed study of the 22 August 2005 landslide and distress on the natural hillside above Kwun Ping Road, Kwun Yam Shan, Shatin. *Landslide study report LSR 5/2007*, Geotechnical Engineering Office, Civil Engineering and Development Department, The Government of the Hong Kong Special Administrative Region, Hong Kong, People's Republic of China
- McDougall S (2006) A new continuum dynamic model for the analysis of extremely rapid landslide motion across complex 3D terrain. PhD thesis, University of British Columbia, Vancouver, B.C., Canada, 253 pages
- McDougall S, Hungr O (2004) A model for the analysis of rapid landslide run out motion across three dimensional terrain. *Can Geotech J* 41:1084–1097

- Monaghan JJ, Cas RF, Kos A, Hallworth M (1999) Gravity currents descending a ramp in a stratified tank. *J Fluid Mech* 379:36–39
- Monaghan JJ, Kos A, Issa N (2003) Fluid motion generated by impact. *J Waterw Port Coastal Ocean Eng* 129:250–259
- Norem H, Irgens F, Schieldrop B (1987) A continuum model for calculating avalanche velocities. In: Salm B, Gubler H (eds) *Avalanche formation, movements and effects*. IAHS Publication no. 162. IAHS, Institute of Hydrology, Wallingford, pp 363–379
- Norem H, Irgens F, Schieldrop B (1989) Simulation of snow-avalanche flow in run-out zones. *Ann Glaciol* 13:218–225
- Pastor M, Quecedo M, Fernández Merodo JA, Herreros MI, Gonzalez E, Mira P (2002) Modelling tailings dams and mine waste dumps failures. *Geotechnique* 52:579–591
- Pastor M, Quecedo M, González E, Herreros I, Fernández Merodo JA, Mira P (2004) A simple approximation to bottom friction for Bingham fluid depth integrated models. *J Hydraul Eng ASCE* 130(2):149–155
- Pastor M, Fernández Merodo JA, Herreros MI, Mira P, González E, Haddad B, Drempetic V (2008) Mathematical, constitutive and numerical modelling of catastrophic landslides and related phenomena. *Rock Mech Rock Eng* 41(1):85–132
- Pastor M, Haddad B, Sorbino G, Cuomo S, Drempetic V (2009a) A depth-integrated coupled SPH model for flow-like landslides and related phenomena. *Int J Numer Anal Methods Geomech* 33:143–172
- Pastor M, Blanc T, Pastor MJ (2009b) A depth-integrated viscoplastic model for dilatant saturated cohesive-frictional fluidized mixtures: application to fast catastrophic landslides. *J Non-Newtonian Fluid Mech* 158:142–153
- Pelanti M, Bouchut F, Mangeney A (2008) A Roe-type scheme for two-phase shallow granular flows over variable topography. *ESAIM Math Model Numer Anal* 42(05):851–885
- Peraire J, Vahdati M, Morgan K, Zienkiewicz OC (1987) Adaptive remeshing for compressible flow computations. *J Comput Phys* 72(2):449–466
- Pinyol NM, Alonso EE (2010) Criteria for rapid sliding. II.: thermo-hydro-mechanical and scale effects in Vaiont case. *Eng Geol* 114:211–227
- Pitman EB, Le L (2005) A two-fluid model for avalanche and debris flows. *Philos Trans A Math Phys Eng Sci* 363:1573–1601
- Pudasaini SP (2012) A general two-phase debris flow model. *J Geophys Res* 117, F03010. doi:10.1029/2011JF002186
- Pudasaini SP, Hutter K (2007) *Avalanche dynamics: dynamics of rapid flows of dense granular avalanches*. Springer, Berlin Heidelberg
- Quecedo M, Pastor M (2003) Finite element modelling of free surface flows on inclined and curved beds. *J Comput Phys* 189(1):45–62
- Quecedo M, Pastor M, Herreros MI (2004) Numerical modelling of impulse wave generated by fast landslides. *Int J Numer Methods Eng* 59:1633–1656. doi:10.1002/nme.934
- Roche O, Montserrat S, Niño Y, Tamburrino A (2008) Experimental observations of water-like behavior of initially fluidized, dam break granular flows and their relevance for the propagation of ash-rich pyroclastic flows. *J Geophys Res* 113, B12203. doi:10.1029/2008JB005664
- Russell AR, Wood DM, Kikumoto M (2009) Crushing of particles in idealised granular assemblies. *J Mech Phys Solids* 57(8):1293–1313
- Savage SB, Hutter K (1989) The motion of a finite mass of granular material down a rough incline. *J Fluid Mech* 199:177–215
- Savage SB, Hutter K (1991) The dynamics of avalanches of granular materials from initiation to run-out. Part I: analysis. *Acta Mech* 86:201–223
- Schneider D, Huggel C, Haerberli W, Kaitna R (2011) Unravelling driving factors for large rock-ice avalanche mobility. *Earth Surf Process Landf* 36:1948–1966
- Sosio R, Crosta G, Hungr O (2008) Complete dynamic modeling calibration for the Thurwieser rock avalanche (Italian Central Alps). *Eng Geol* 100(1–2):11–26
- Sosio R, Crosta GB, Hungr O (2011) Numerical modeling of debris avalanche propagation from collapse of volcanic edifices. *Landslides* 9:315–334
- Sosio R, Crosta GB, Chen JH, Hungr O (2012) Modelling rock avalanche propagation onto glaciers. *Quat Sci Rev* 47:23–40
- Taboada A, Estrada N (2009) Rock-and-soil avalanches: theory and simulation. *J Geophys Res* 114, F03004. doi:10.1029/2008JF001072
- Takahashi T, Nakagawa H, Harada T, Yamashiki Y (1992) Routing debris flows with particle segregation. *J Hydraul Eng* 118(11):1490–1507
- Toro EF (2001) *Shock-capturing methods for free-surface shallow flows*. Wiley, New York
- Trujillo L, Herrmann HJ (2003) Hydrodynamic model for particle size segregation in granular media. *Phys A Stat Mech Appl* 330(3):519–542
- Vallance JW, SB Savage (2000) Particle segregation in granular flows down chutes. In: Rosato AD, Blackmore DL (eds) *Solid mechanics and its applications*. IUTAM Symposium on Segregation in Granular Flows. Springer, pp. 31–51
- Voellmy A (1955) Über die Zerstörungskraft von Lawinen. *Schweiz Bauzeitung* 73:159–165, 212–217, 246–249, 280–285
- Zienkiewicz OC, Shiomi T (1984) Dynamic behaviour of saturated porous media: the generalised Biot formulation and its numerical solution. *Int J Numer Analytical Methods Geomech* 8:71–96
- Zienkiewicz OC, Chang CT, Bettess P (1980) Drained, undrained, consolidating dynamic behaviour assumptions in soils. *Geotechnique* 30:385–395
- Zienkiewicz OC, Chan AHC, Pastor M, Paul DK, Shiomi T (1990a) Static and dynamic behaviour of soils: a rational approach to quantitative solutions. I. Fully saturated problems. *Proc R Soc (London) A* 429:285–309
- Zienkiewicz OC, Xie YM, Schrefler BA, Ledesma A, Bicanic N (1990b) Static and dynamic behaviour of soils: a rational approach to quantitative solutions. II. Semi-saturated problems. *Proc R Soc (London) A* 429:311–321
- Zienkiewicz OC, Chan AHC, Pastor M, Shrefler BA, Shiomi T (2000) *Computational geomechanics*. Wiley, Hoboken

M. Pastor (✉) · **T. Blanc** · **B. Haddad** · **S. Petrone** · **M. Sanchez Morles** · **V. Drempetic**

Mathematical Modelling in Engineering Group (M2i), Department of Applied Mathematics and Computer Science, ETS Ingenieros de Caminos, Universidad Politécnica de Madrid, Madrid, Spain
e-mail: manuel.pastor@upm.es

D. Issler

Norwegian Geotechnical Institute and International Centre for Geohazards, Oslo, Norway

G. B. Crosta

Department of Earth and Environmental Sciences, Università degli Studi di Milano Bicocca, Milan, Italy

L. Cascini · **G. Sorbino** · **S. Cuomo**

University of Salerno, Salerno, Italy